



Doctoral Thesis in Engineering Mechanics

Numerical predictions of heat-transfer applied to electrical machines

KRISTIAN RÖNNBERG

Numerical predictions of heat-transfer applied to electrical machines

KRISTIAN RÖNNBERG

Academic Dissertation which, with due permission of the KTH Royal Institute of Technology, is submitted for public defence for the Degree of Doctor of Philosophy on Thursday the 15th December 2022, at 1:00 p.m. in H1, Teknikringen 33, Stockholm.

Doctoral Thesis in Engineering Mechanics
KTH Royal Institute of Technology
Stockholm, Sweden 2022

- © Kristian Rönnerberg
- © Kristian Rönnerberg, Minos Beniakar, Paper 1
- © Kristian Rönnerberg, Christophe Duwig, Paper 2
- © Kristian Rönnerberg, Christophe Duwig, Paper 3
- © Kristian Rönnerberg, Panagiotis Kakosimos, Zlatko Kolondjovski, Erik Nordlund, Paper 4
- © Kristian Rönnerberg, Zlatko Kolondjovski, Christophe Duwig, Paper 5

ISBN 978-91-8040-427-3
TRITA-SCI-FOU 2022:60

Printed by: Universitetservice US-AB, Sweden 2022

Kristian Rönnerberg

Division of Process Technology, KTH Royal Institute of Technology, Department of Chemical Engineering
SE-100 44 Stockholm, Sweden

Abstract

In order to meet the need for increased electrification, and at the same time reduce the total demand for electric energy, behavior change and technological innovation is needed. Over the decades power density of electric motors have increased, leading to increased demands on the cooling system design and performance. The need for reduced energy demand, increased efficiency, and continued increase in performance require continuous development effort regarding cooling systems, understanding of temperature distributions and heat transfer, and thermal simulation tools applicable in the motor manufacturing industry.

A study on how simulation assumptions affect the resolved temperature field in a traction motor prototype is presented. Here different assumptions regarding loss distributions and air flow distributions are considered. The study illustrates how different simulation assumptions affect the temperature field, and how the results compare to measurements.

Application of numerical methods for resolving heat transfer, and how the heat transfer is linked to features in the fluid flow, is presented. An air jet impinging on a heated surface is investigated through the application of Large Eddy Simulations (LES) and obtained data processed using the Extended Proper Orthogonal Decomposition (EPOD) method. The study shows the link between structures in the flow and the associated structures in heat transfer.

Thermal analysis is an integral part of the motor design and dimensioning process. The method employed in these studies is often the Lumped Parameter Thermal Network (LPTN). In this work a prototype method for automatic calibration of an LPTN, based on external temperature data, is presented. Application of Computational Fluid Dynamics (CFD) in computing input data needed for LPTNs is presented, where an extension to existing heat transfer correlations related to the end-winding of a form-wound machine is suggested.

The studies are aiming at enabling advancing the prediction capability of heat transfer and temperature simulation methods applied in analysis of electrical machines.

Key words: Electric machines, energy efficiency, heat transfer, thermal management, high fidelity simulation, computational fluid dynamics (CFD), proper orthogonal decomposition (POD), lumped parameter thermal network (LPTN)

Numerisk analys av värmeöverföring tillämpad på elektriska maskiner

Kristian Rönnerberg

Processteknologi, Kungliga Tekniska Högskolan, Kemiteknik
SE-100 44 Stockholm, Sverige

Sammanfattning

För att möta behovet av utökad elektrifiering, samtidigt som energibehovet behöver reduceras, krävs både beteendeförändringar och teknologisk innovation. Effekttätheten i roterande maskiner har ökat under decennierna, vilket leder till förhöjda krav på kylningssystemens utformande och prestanda. Kombinationen av behovet av minskning av energibehov, höjd verkningsgrad samt ökade prestandakrav, kräver kontinuerlig utveckling av kylsystem, förståelse av temperaturfördelning och värmeöverföring, samt simuleringsverktyg tillämpbara i motortillverkningsindustrin.

En studie av hur antaganden i definieringen av simuleringar påverkar den erhållna temperaturprofilen presenteras i denna avhandling. Studien utfördes med utgångspunkt från en traktionsmotorprototyp. Olika antaganden gällande förlustfördelning och fördelning av kylflöde beaktades. Studien illustrerar hur olika antaganden påverkar det simulerade temperaturfältet, och hur resultaten står sig i jämförelse med mätningar.

Numeriska metoder för upplösning av värmeöverföring och hur denna är kopplad till strukturer i fluiden presenteras. En luftstråle som infaller på en uppvärmd plan yta studerades med hjälp av Large Eddy Simulation (LES) och erhållna data behandlades med Extended Proper Orthogonal Decomposition (EPOD). Studien visar på kopplingen mellan strukturer i flödet och strukturer i värmeöverföringen.

Termisk analys är en viktig del av design- och dimensioneringsprocessen för en motor. En vanligt förekommande metod för detta är termiska nätverk. I denna avhandling presenteras en prototyp till en metod för automatisk kalibrering av termiska nätverk, där kalibrering sker mot en extern källa till temperaturdata. Tillämpning av Computational Fluid Dynamics (CFD) för att beräkna in-data till termiska nätverk presenteras också, där en utökning av befintliga korrelationer för värmeöverföring vid lindningsutsticken hos formlindade maskiner föreslås.

Studierna ämnar till att möjliggöra förbättra predikteringsförmågan hos värmeöverförings- och temperatursimuleringsmetoder tillämpade vid analys av elektriska maskiner.

Nyckelord: Elektriska maskiner, energieffektivitet, verkningsgrad, värmeöverföring, värmehantering, simuleringar med hög upplösning, strömmingsmekaniska beräkningar, proper orthogonal decomposition (POD), termiska nätverk

Preface

This thesis deals with heat-transfer simulations applied to electrical machines. A brief introduction on the basic concepts and methods is presented in the first part. The second part contains three articles. The papers are adjusted to comply with the present thesis format for consistency, but their contents have not been altered as compared with their original counterparts.

Paper 1. K. RÖNNBERG & M. E. BENIAKAR, 2018. *Thermal Modelling of Totally Enclosed Fan Cooled motors*. XIII International Conference on Electrical Machines (ICEM), 2619–2625.

Paper 2. K. RÖNNBERG & C. DUWIG, 2019. *Large Eddy Simulation of circular impinging jet for heat transfer applications*. Direct and Large Eddy Simulation XII **27**, 69–75.

Paper 3. K. RÖNNBERG & C. DUWIG, 2021. *Heat transfer and associated coherent structures of a single impinging jet from around nozzle*. International Journal of Heat and Mass Transfer **173**, 121197.

Paper 4. K. RÖNNBERG, P. KAKOSIMOS, Z. KOLONDOVSKI, E. NORDLUND, 2022. *Machine Learning-Based Adjustments Of Thermal Networks*. The 11th International Conference on Power Electronics, Machines and Drives 2022 (PEMD).

Paper 5. K. RÖNNBERG, Z. KOLONDOVSKI, C. DUWIG, 2022. *Analysis of end winding heat transfer in a low-speed motor with forced external cooling*. Submitted to IEEE Transactions on Energy Conversion.

November 2022, Munktorp
Kristian Rönnerberg

Division of work between authors

The main advisor for the project is Christophe Duwig (CD). Anders Dahlkild and Luca Peretti act as co-advisors. Advisor from the industrial partner was Rebei Bel-Fdhila between 2017 and 2020, and Zlatko Kolondjovski from 2020 until completion.

Paper 1. Kristian Rönnerberg: Conceptualization, Formal analysis, Investigation, Data Curation, Writing - Original Draft, Writing - Review & Editing, Visualization. **Minos Beniakar:** Conceptualization, Investigation, Writing - Original Draft, Writing - Review & Editing, Visualization.

Paper 2. Kristian Rönnerberg: Conceptualization, Methodology, Formal analysis, Investigation, Data Curation, Writing - Original Draft, Writing - Review & Editing, Visualization. **Christophe Duwig:** Conceptualization, Methodology, Writing - Review & Editing, Supervision, Funding acquisition.

Paper 3. Kristian Rönnerberg: Conceptualization, Methodology, Formal analysis, Investigation, Data Curation, Writing - Original Draft, Visualization. **Christophe Duwig:** Conceptualization, Methodology, Writing - Review & Editing, Supervision, Funding acquisition.

Paper 4. Kristian Rönnerberg: Conceptualization, Methodology, Formal analysis, Investigation, Data Curation, Writing - Original Draft, Writing - Review & Editing, Visualization. **Panagiotis Kakosimos:** Conceptualization, Writing - Original Draft. **Zlatko Kolondjovski:** Methodology, Writing - Original Draft. **Erik Nordlund:** Conceptualization, Methodology, Writing - Original Draft, Project administration

Paper 5. Kristian Rönnerberg: Conceptualization, Methodology, Formal analysis, Investigation, Data Curation, Writing - Original Draft, Writing - Review & Editing, Visualization. **Zlatko Kolondjovski:** Conceptualization, Validation, Writing - Original Draft. **Christophe Duwig:** Writing - Original Draft, Supervision, Funding acquisition

Other publications

The following papers, although related, are not included in this thesis.

SOMAYEH MALAKUTI, REUBEN BORRISON, ARZAM KOTRIWALA, BENJAMIN KLOPPER, ERIK NORDLUND, KRISTIAN RÖNNBERG, 2021. *An Integrated Platform for Multi-Model Digital Twins*. 11th International Conference on the Internet of Things (IoT '21), pp. 6–19.

Contents

Abstract	iii
Sammanfattning	iv
Preface	v
Nomenclature	xi
Part I - Overview and summary	
Chapter 1. Introduction	1
1.1. Aim of the work	2
1.2. Scope of work	2
1.3. Scientific contribution	3
Chapter 2. Electric machines	5
2.1. Power output density over the years	5
2.2. Electric machine types and topologies	6
2.3. Losses and heat sources in machines	7
2.4. Cooling arrangements and methods	11
2.5. Relative importance of heat transfer coefficient at the end winding of a form wound machine	13
2.6. Selected area for research	18
Chapter 3. Fluid mechanics and heat transfer theory	19
3.1. Sources of qualitative information	19
3.2. Governing equations - Compressible flow	19
3.3. Governing equations - Incompressible flow	23
3.4. Dimensionless numbers	25
Chapter 4. Methods	29
4.1. Thermal and fluid flow simulations	29

4.2. Model order reduction	33
Chapter 5. Investigations	35
5.1. Considerations for temperature measurements on lab scale setups (Paper 1)	35
5.2. Computational methods to use for introducing new cooling features (Papers 2 & 3)	38
5.3. New features for design tools (Papers 4 & 5)	38
Chapter 6. Conclusions and outlook	41
Acknowledgements	43
Bibliography	44

Part II - Papers

Summary of the papers	51
Paper 1. Thermal Modelling of Totally Enclosed Fan Cooled motors	53
Paper 2. Large Eddy Simulation of circular impinging jet for heat transfer applications	63
Paper 3. Heat transfer and associated coherent structures of a single impinging jet from a round nozzle	71
Paper 4. Machine Learning-Based Adjustments Of Thermal Networks	87
Paper 5. Analysis of end winding heat transfer in a low-speed motor with forced external cooling	95

Nomenclature

The list of symbols and numbers refer to their use and meaning in Part I. The papers presented in Part II contain separate definitions of symbols used.

Acronyms

CAD	Computer-aided Design
CFD	Computational Fluid Dynamics
CHT	Conjugate Heat Transfer
DAE	Differential Algebraic Equation
EPOD	Extendend Proper Orthogonal Decomposition
FDM	Finite Difference Method
FEM	Finite Element Method
FVM	Finite Volume Method
IEA	International Energy Agency
IPCC	Intergovernmental Panel on Climate Change
LCA	Life Cycle Assessment
LES	Large-Eddy Simulation
LPTM	Lumped Parameter Thermal Model
LPTN	Lumped Parameter Thermal Network
MOR	Model Order Reduction
ODE	Ordinary Differential Equation
PDE	Partial Differential Equation
POD	Proper Orthogonal Decomposition
RANS	Reynolds-averaged Navier-Stokes
VSD	Variable Speed Drive

Greek symbols

α	Thermal diffusivity ($\text{m}^2 \text{s}^{-1}$) [= $\kappa/(\rho \cdot c_p)$]
δ_{ij}	Kroenecker delta function. 0 if $i \neq j$, 1 if $i = j$
η	Heat transfer coefficient ($\text{W m}^{-2} \text{K}^{-1}$)
κ	Thermal conductivity ($\text{W m}^{-1} \text{K}^{-1}$)
λ	Second coefficient of viscosity
$\lambda^{(n)}$	Eigenvalue of mode order n
μ	Dynamic viscosity (Pa·s)
μ_t	Turbulent dynamic viscosity (Pa·s)

ν	Kinematic viscosity ($\text{m}^2 \text{s}^{-1}$) [= μ/ρ]
$\Phi_i^{(n)}$	POD spatial basis function of mode order n of vector component i
$\Psi_i^{(n)}$	EPOD spatial basis function of mode of order n of vector component i
ρ	Density (kg m^{-3})
ζ	Volume viscosity (Pa·s)

Latin symbols

\dot{q}_W	Constant heat flux boundary condition
$a^{(n)}$	Time coefficient of mode order n
C	Courant number
c	Speed of sound (m s^{-1})
c_p	Specific heat at constant pressure ($\text{J kg}^{-1} \text{K}^{-1}$)
c_v	Specific heat at constant volume ($\text{J kg}^{-1} \text{K}^{-1}$)
f	Frequency (Hz)
h	Enthalpy (J)
l	Characteristic length (m)
p	Pressure (Pa)
T	Temperature (K)
t	Time (s)
u	Velocity i (m s^{-1})
u_i	Velocity component i (m s^{-1})
x_i	Cartesian coordinate i (m s^{-1})

Non-dimensional numbers

Bi	Biot number
Kn	Knudsen number
Le	Lewis number
Ma	Mach number
Nu	Nusselt number
Pe	Peclet number
Pr	Prandtl number
Re	Reynolds number
Sc	Schmidt number
Sr	Strouhal number
Stk	Stokes number

Part I

Overview and summary

Introduction

Both the International Energy Agency (IEA) and the Intergovernmental Panel on Climate Change (IPCC) emphasize that behavioral and technological changes are needed for the world to come to a sustainable trajectory (IEA (2021 *a,b*); IPCC (2022)). On the technological side, new innovations, continued implementation of low-emission technology, energy efficiency measures and energy efficiency improvements to existing technology are needed. Motors in industry constitute a large part of the demand for electric energy, around 30 % (9346 TWh) of total electricity demand (23031 TWh) in 2018 according to IEA (2019). Share of demand is not expected to grow in the future scenarios outlined in IEA (2019), but net energy demand from industrial motors will increase to 11418 TWh by 2040 if development proceeds according to the stated policies from when the report was written. In order to align with the Sustainable Development Scenario (SDS) described in the same report, this demand increase by 2040 need to be reduced to reach a total energy demand from motor driven systems of 9290 TWh. Due to this it is of high relevance to continue to push for improvements, on individual motor level and on powertrain¹ level, that have positive influence on energy efficiency.

For assessments on environmental footprint of a product, all steps from manufacturing to end-of-life need to be consider. In a Life Cycle Assessment (LCA) of a selection of motors presented by Orlova *et al.* (2016), the contribution to the environmental footprint was found to be close to 99% from the use phase, due to the energy consumption. The remaining 1% of the environmental footprint stems from manufacturing and disposal. Energy efficiency improvements on motor level thus have a large influence on the total environmental footprint of an electric motor.

At the design phase of an electric motor there is a tight link between the electromagnetic and thermal performance characteristics. The motor should deliver torque and power to fulfill the intended application, at as high efficiency as possible, while being constructed from as little, active² and in-active, material

¹In this context a powertrain is envisioned to consist of a supply, such as a frequency converter, a motor and a load.

²Active material is typically a designation given to current carrying (commonly copper and aluminium) and magnetic flux guiding material (electrical steel).

as possible. At the same time, it needs to be "large enough" to accommodate a suitable cooling system, which itself need to be well-dimensioned. Efficiency improvements in the electromagnetic design could thus result in the need for a smaller cooling system, and increased heat transfer may allow for use of less active material or less losses due to operation at a lower temperature level³. Thus, heat transfer related topics are an integral aspect of electric machine design and play a role in efficiency improvement efforts.

There are reports by authors such as Capehart *et al.* (2020), Saidur (2010) and Bortoni (2009) that oversized motors are commonly found in installations and that oversizing has an adverse effect on the energy efficiency. In driving energy efficiency improvements it can thus be expected that more well-sized motors will be found in installations going forward. This will make cooling and dimensioning based on thermal management questions even more relevant, as there will be less operational thermal margin compared to in an oversized machine.

Energy efficiency improvements have the potential to reduce expenses for equipment owners and are expected to be considered as a part of maintenance and refurbishment plans. At the same time new energy efficiency directives are being put in place ensuring that energy efficiency is a topic in focus. A recent example of this are the European Union (EU) eco-design requirements found in EU C/2019/2125 (2019-10-25). For motor manufacturers to keep improving the efficiency of their products and systems, all parts will be considered for improvements. Including cooling features and systems.

1.1. Aim of the work

One aim of this work is to investigate the applicability of different numerical methods for studying heat transfer in rotating electrical machines. The intention is that the investigated methods can be used in product development for improving material efficiency, energy efficiency, and machine performance. Another aim is to apply methods for obtaining new data and understanding of heat transfer in rotating electrical machines. In the papers associated with this thesis different methods have been employed to study or explore phenomena and aspects associated with heat transfer for different systems. Their applicability in electric machine development will be discussed in this thesis.

1.2. Scope of work

This work considers the application of numerical methods and simulations that can be applied in heat transfer studies of electrical machines. The machine types studied are radial flux machines, typically designed for being supplied by power through a Variable Speed Drive (VSD). This implies that the machines are intended for operation at varying speeds. Furthermore, the machines considered are not in the high speed range, and the machine with the highest permissible

³Resistive losses in conductors decrease with decreasing temperature.

speed has a maximum speed of a few thousand rpm at most. The primary coolant considered in the studies is air. Conventional methods for motor thermal analysis, the Lumped Parameter Thermal Network (LPTN), is considered, in addition to numerical methods that can render higher resolution of air flow phenomena. For air flow studies the Finite Volume Method (FVM) is employed. Generators are not explicitly considered among the specimens, as the main focus is on the electrical load demand side. The methods considered are however applicable for studying generators as well.

1.3. Scientific contribution

Thermal simulations of electric machines are often compared to measurements performed at specific locations with temperature sensors mounted at locations that cannot be reached after assembly. How well the measurements and simulations compare depend on assumptions made during definition of the simulations setup. Studies on how simulation assumptions affect the computed temperature field inside electric machines, and how the results compare to measurements, are not common. The work covered in this thesis contributes a study of this question, which can aid future experimental setups intended for thermal model development and evaluation.

Numerical methods for studying and understanding heat transfer are of high relevance for electric machine analysis. High fidelity numerical methods were applied for understanding the link between structures in the fluid flow and heat transfer in the canonical configuration of an impinging jet. In this work, Extended Proper Orthogonal Decomposition was employed on data obtained through Large Eddy Simulations (LES), for what appears to be the first time, to study this connection.

Definition of lumped parameter thermal network models for electric machines requires calibration using experimentally obtained results. The calibration process is needed as the manufacturing tools and processes affect the thermal performance of the completed machine. Additionally, during introduction of modifications to features affecting heat transfer calibrations of thermal models are needed. Available literature focus on the experiments to perform for obtaining data for calibration. In the work covered in this thesis, a method for automating the adjustment of the lumped parameter thermal model definition based on temperature data input is prototyped. Such a method can be applied in an industrial context for obtaining calibrated thermal models.

Many electric motors have the internal air flow driven solely by the rotor rotation. Given how common this driver of internal air flow is, heat-transfer correlations for this type of internal air flow can be found in literature. For certain high-performance applications an external cooling system which provide forced cooling may be employed. Heat-transfer studies of the end-winding for this type of cooling system is not common in literature and no correlations were found published. In the work considered in this thesis, a heat-transfer

correlation for the end-winding region is presented. The presented correlation is suitable for implementation in design tools.

Thesis structure. The thesis is divided into two parts, the first part is an overview of the work performed, and the second part contains the attached papers. The first part contains six chapters. Chapter 1: Introduction (this chapter) introduces the need for the work, background and contribution. Chapter 2: Electric machines gives a short introduction to electric machines, types, heat sources, cooling methods, and area for research. Chapter 3: Fluid mechanics and heat transfer theory briefly introduces equations describing compressible and incompressible fluid flow, together with some useful non-dimensional numbers. Chapter 4: Methods gives an introduction to selected methods for thermal analysis employed in rotating machine analysis, and selected methods associated with model order reduction. Chapter 5: Investigations presents the investigations compiled into papers. Finally, Chapter 6: Conclusions and outlook summarizes the studies and relates them to the area for research selected, and finally presents some outlook.

Electric machines

This chapter contains an introduction to cooling methods for rotating electric machines. The link between cooling need and methods is illustrated by the increase in power output from electric motors over the last century.

2.1. Power output density over the years

The rotating electric machine (motor or generator) has been around for more than a century. During this time the power output per unit mass has increased significantly, which is illustrated in Figure 2.1. This development was made

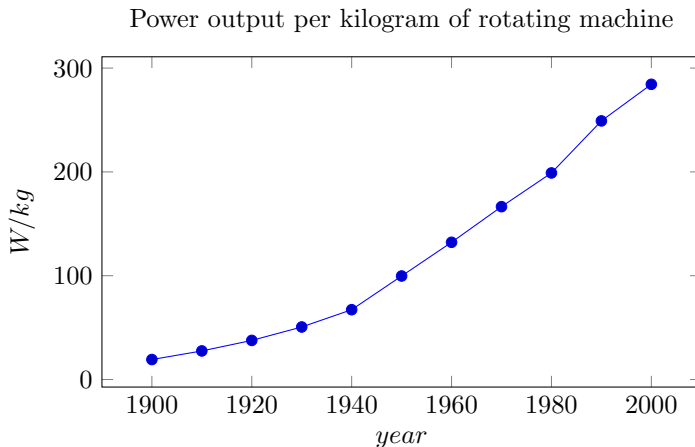


Figure 2.1: Power output per kilogram of rotating machine. Figure data from Stone *et al.* (2014). Original data from Glew (1999).

possible by e.g. new insulation materials and new manufacturing methods introduced according to Stone *et al.* (2014). As is explained in Lipo (2017), the total cooling area of a machine is proportional to the square of a representative machine dimension (length or diameter). Therefore, a machine with roughly the same exterior dimensions would require a higher intensity heat removal when

increasing output power per mass from early 1900 levels to year 2000 levels, under the simplifying assumption that power conversion efficiency ($\eta = P_{out}/P_{in}$) has remained the same throughout the century. This increase in material utilization clearly illustrates the need for work on cooling features and systems.

2.2. Electric machine types and topologies

There are several ways to classify and group electric machines: based on the type of motion as in *rotary* or *linear* machines, based on the type of supply as AC or DC machine, based on type of AC supply as in Direct On-Line (DOL) or Variable Speed Drive (VSD) machine, based on if the machine is rotating synchronously or asynchronously with the supply frequency, based on the rotor construction as in Surface mounted Permanent Magnet (SPM) or Interior Permanent Magnet (IPM), based on how the magnetic flux density is aligned with the axis of rotation as in axial and radial flux machines, based on the stator winding type as in form winding or random winding, based on how the winding is arranged in the stator as in concentrated or distributed winding, or based on the type of motion the machine is experiencing as in linear or rotary machines. Which classification is used depends on the context and machine properties of interest; In the work by Bolam *et al.* (2018) the motors are group into *DC motors (Brushed)*, *Switched Reluctance Motors*, *Induction Motors*, *AC Synchronous Motors* and *Brushless DC Motors (BLDC)*; In the work by Kahourzade *et al.* (2014) the machines are identified by very specific details related to Axial Flux Permanent Magnet (AFPM) machines; and in the work by Ballestín-Bernad *et al.* (2021) based on the flux density direction as in Radial Flux Machines (RFM), Axial Flux Machines (AFM), and Transverse Flux Machines (TFM).

The rotating radial flux machine is the most common machine type for industrial applications, such as driving pumps, fans, and conveyor belts. It is also commonly found in rail propulsion systems in everything from trams to high speed rail applications. The theory behind the rotating radial flux machine is described in books by e.g. Pyrhonen *et al.* (2014) and Lipo (2017). Linear machine theory is described in e.g. the book by Boldea (2013), from which it can be found that an example of a linear machine is the propulsion system found in MAGLEV (magnetic levitation) trains.

The machines considered in this thesis, specifically in **paper 1**, **paper 4**, and **paper 5** are all of the rotary radial flux type. In **paper 1** a synchronous machine with interior permanent magnets in the rotor is the subject of study, **paper 4** considers a subset of a generic stator found in radial flux machines, and **paper 5** considers the end winding region of an induction machine (asynchronous machine) with form windings in the stator. Given the focus on radial flux machines, all example illustrations in subsequent sections are based on rotary radial flux machines.

2.3. Losses and heat sources in machines

Losses in rotating electric machines are commonly divided into (see e.g. Lipo (2017); Pyrhonen *et al.* (2014); Krings (2014)): *mechanical losses*, *iron losses* or *core losses*, *resistive losses*, and *additional losses* or *stray-load losses*. When the machine is supplied from a converter, a loss component referred to as *harmonic loss* can be introduced (Aarniovuori *et al.* (2018)). The iron losses, P_{iron} , arise due to the alternating magnetic flux density in the flux guiding materials, which are typically an electrical steel. The resistive losses, $P_{resistive}$, are found in the current carrying features of the machines such as the stator winding, rotor winding or rotor bars. Mechanical losses, P_{mech} , are associated with losses in bearings, friction losses due to air flow and the power required to drive necessary cooling air flows. The *additional losses*, $P_{add.}$, are used to account for the difference between estimated and measured losses. Total losses, P_{loss} , are the difference between the input power, P_{in} (electrical input power in the case of a motor), and the output power P_{out} (mechanical power in the case of a motor). The total loss is illustrated by eq. (2.1), additional loss by eq. (2.2) and the estimated loss by eq. (2.3). An illustration of where these losses occur is found in Figure 2.2. The 2D cross section shown is representative of a low voltage induction machine for industrial applications.

$$P_{in} - P_{out} = P_{loss} = P_{mech} + P_{iron} + P_{resistive} + P_{add.} \quad (2.1)$$

$$P_{meas} - P_{est.} = P_{add.} \quad (2.2)$$

$$P_{est.} = P_{mech} + P_{iron} + P_{resistive} \quad (2.3)$$

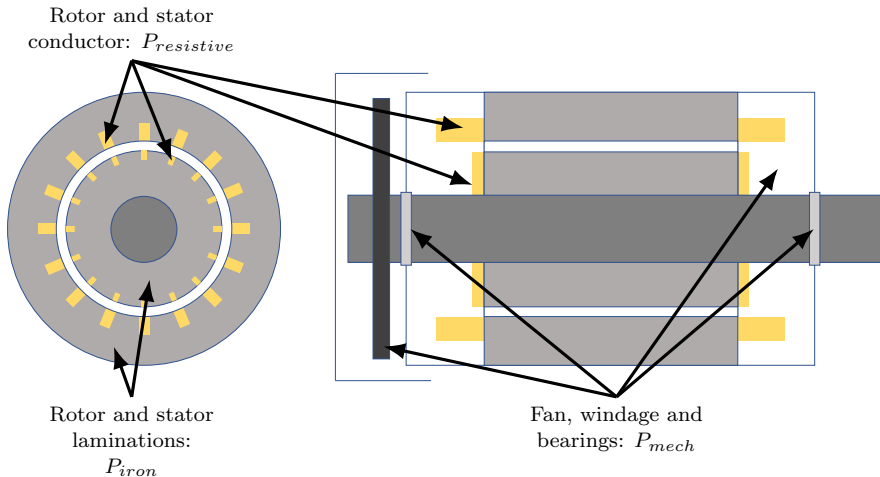


Figure 2.2: 2D cross section principle illustration of a low voltage induction machine for industrial applications.

The relative size of the different loss terms differ depending on machine type, speed and topology. The distribution in three different types of machines; a 110kW high speed permanent magnet (PM) generator, a 11kW induction machine (IM), and a 1kW slot-less PM motor for hand tools were presented by Krings (2014). The data is adapted and presented in Figure 2.3. What is clear from this figure is that the dominating loss source differs and that an application-by-application analysis is necessary for understanding which part to cool and how.

An in-depth analysis of losses and loss components in induction motors for industrial applications, with rated power in the range 7.5 to 355 kW, can be found in the work by Aarniovuori *et al.* (2018).

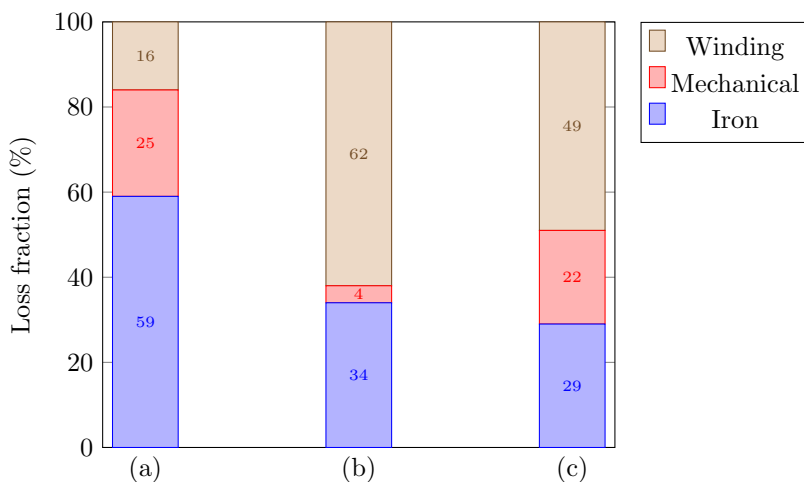


Figure 2.3: Fraction of total loss per loss type in different machine types. (a) 110kW, 51 krpm, PM generator, (b) 11kW, 1470 rpm, IM, (c) 1kW, 36 krpm, slot-less PM motor. Data adapted from Krings (2014).

If the machine is equipped with rolling-element bearing, which are typically mass produced by large and knowledgeable bearing suppliers, the mechanical losses associated with the bearing can often be estimated based on supplier data or supplier formulas. In some large machines with heavy rotors fluid bearings can often be found. These require individual analysis depending on application for accurate loss estimation.

The windage loss is highly dependent on motor topology and associated design. In this context *windage loss* refers to the power that goes to driving flow in and around the machine. There are several design aspects that affect the windage loss; presence of shaft driven fans, cooling ducts, presence of rotor-mounted wafers, cowling design etc. While there are analytical formulas

for estimating windage loss in machine, as those presented in Pырhonen *et al.* (2014), they are often based on canonical geometries (such as rotating cylinders etc.). It is thus challenging to apply them for accurate and reliable predictions. Lipo (2017) mentions that measurements are the most reliable way to determine the windage loss.

Resistive losses in current-carrying parts can be computed based on various forms of I^2R , where I is the current and R is the resistance. Depending on the application R may contain purely material and geometric parameters, or it may include coefficients to include effects associated with alternating current phenomena such as skin effects and un-even current distributions. For an introduction to these topics it is best to consult e.g. Lipo (2017) or Pырhonen *et al.* (2014).

The iron losses are a result of material properties (steel grade), the exciting current waveform, local flux density magnitude, and the local flux density variation. The method and tools used for shaping the steel, e.g. punching or laser cutting, into suitable form for use as part of a stator or rotor also influences the loss levels. An overview of the principles of manufacturing, post-production treatment, properties to consider, and more, is given by Beckley (2002) and Moses *et al.* (2019a). Due to the many factors affecting the total iron loss it poses a challenge for predictions. Several models have been developed for prediction of iron losses. An overview of such methods and the considerations behind them are presented by Krings & Soulard (2010). The overview also presents the material data detail needed for using the different methods. One model mentioned by Krings & Soulard (2010), which requires a medium level of material data, is based on dividing the total loss into components due to eddy currents, hysteresis effects and excess losses. In this model the different components are dependent on peak flux density, \hat{B} , and frequency, f , as

$$p_{iron} = p_{hyst} + p_{ec} + p_{exc} = C_{hyst}f\hat{B}^2 + C_{ec}f^2\hat{B}^2 + C_{exc}f^{1.5}\hat{B}^{1.5} \quad (2.4)$$

where the coefficients C_{hyst} , C_{ec} and C_{exc} need to be found by fitting the expression to data from measurements. In the above equation, p_{iron} is the specific iron loss (i.e. iron loss per unit mass), p_{hyst} the specific hysteresis loss, p_{ec} the specific eddy current loss, and p_{exc} the specific excess loss. Measurement data to be used for fitting can e.g. be found in data sheets from electrical steel suppliers. An example of supplier data of an M270-50A steel that was found online (Tata Steel - Surahammars Bruk (2022)) is presented in Table 2.1.

Table 2.1: Example material data of a M270-50A type material. Data adapted from Tata Steel - Surahammars Bruk (2022).

\hat{B} (T)	W/kg at 50Hz	W/kg at 100Hz	W/kg at 200Hz
0.1	0.02	0.04	0.10
0.2	0.07	0.17	0.43
0.3	0.14	0.35	0.91
0.4	0.23	0.58	1.51
0.5	0.33	0.85	2.24
0.6	0.45	1.16	3.09
0.7	0.58	1.51	4.07
0.8	0.73	1.90	5.19
0.9	0.90	2.33	6.47
1.0	1.07	2.81	7.94
1.1	1.27	3.36	9.61
1.2	1.50	3.98	11.50
1.3	1.76	4.71	13.60
1.4	2.13	5.62	16.30
1.5	2.52	6.69	19.20
1.6	2.87		
1.7	3.13		
1.8	3.37		

\hat{B} (T)	W/kg at 400Hz	W/kg at 1000Hz	W/kg at 2500Hz
0.1	0.29	1.40	5.75
0.2	1.15	5.01	20.10
0.3	2.48	10.20	42.40
0.4	4.17	17.20	73.70
0.5	6.24	26.10	116.00
0.6	8.75	37.40	173.00
0.7	11.70	51.40	248.00
0.8	15.20	68.70	344.00
0.9	19.30	89.60	468.00
1.0	24.10	115.00	627.00
1.1	29.70	145.00	
1.2	36.00		
1.3	43.30		
1.4	51.90		
1.5	61.90		
1.6			
1.7			
1.8			

The testing specifications and steel grade naming convention is defined in IEC (2022a). Testing procedures for electrical steel properties are described by Moses *et al.* (2019b). The model is intended for sinusoidal excitation waveforms. However, the semi-conductor based variable speed drive (VSD) which is in use today in everything from industry installations to electric vehicles do not produce a pure sinusoidal waveform. The excitation waveform from a VSD contains harmonics which cause an increase in iron losses (Beckley (2002); Moses *et al.* (2019b)) due to the harmonic content. Illustrations and explanations of this increase in losses are found presented by Moses *et al.* (2019b). Additionally, as is highlighted by Krings & Soulard (2010), the model does not account for losses due to locally rotating fields. Rotational loss is explained in Moses *et al.* (2019a) and Moses *et al.* (2019b).

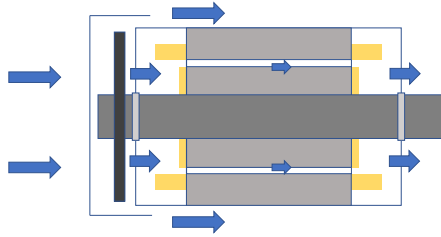
Losses in rotating machines depend on several factors, as indicated above. They depend on the machine topology and design, as this dictates the excitation waveform through e.g. machine inductance and resistance. Given the challenge to predict e.g. core losses, and that this is a field of active research, spatial distributions of losses inside machines are a challenge to estimate. This information is needed for temperature distribution simulations of machines. More thus remains until 3D spatial loss distributions can be obtained. Which is a requirement for obtaining 3D temperature distributions that are fully reflecting the system studied.

2.4. Cooling arrangements and methods

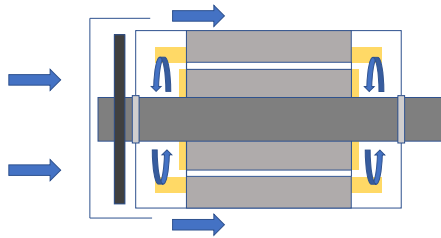
The widespread use of electric motors for everything from material handling to propulsion has naturally lead to variations in topology, design, and supply: from direct-on-line (DOL) DC machines to variable speed drive (VSD) connected permanent magnet assisted synchronous reluctance machines. As losses in the energy conversion process need to be handled, various cooling arrangements have been employed. Several cooling arrangements for industrial motors are for example given a standard designation by the International Electrotechnical Commission (IEC) (IEC (1991)). A comprehensive review of cooling of motors used in electric cars can be found in Wang *et al.* (2022), where also many topics of relevance for machines in industrial applications are mentioned. The machine types of primary focus in this thesis are for industrial applications.

An illustration, based on a radial flux machine, of three common cooling arrangements is found in Figure 2.4. These arrangements are seen on smaller industrial motors and motors for traction applications. The illustrations show a fan attached and driven by the motor shaft, thus rotating at the same speed as the machine. For some applications it is preferred to have control over the fan speed, and in those cases the cooling fan can be driven by a separate fan motor. Different motor manufacturers have their own variants of fans, fan cowlings, cooling fins, etc. The overall principles are though the same.

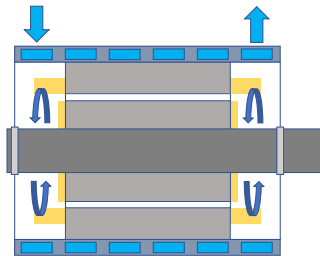
A cooling arrangement which is quite often seen on larger machines is the enclosed motors with a heat exchanger. Here the same cooling fluid is circulated



(a) Open self-ventilated: Air flow is driven by a shaft-mounted fan and the machine ends are open, allowing ambient air to pass through the machine.



(b) Totally enclosed fan cooled (TEFC): External air flow is driven by a shaft-mounted fan. The machine is sealed so ambient air is separated from internal air. Internal air flow is driven by the rotor.



(c) Water jacket: The machine is cooled by water passing through a water jacket attached to the frame. Internal air flow is driven by the rotor.

Figure 2.4: Sketches of common cooling arrangements found on smaller industrial motors and traction motors.

inside the machine, and the cooling fluid is in turn cooled through a heat exchanger. This heat exchanger can have air or water on the secondary side (with the primary side being exposed to the fluid in the machine). This type of arrangement is illustrated for a machine with a symmetric cooling circuit in Figure 2.5. The term symmetric refers to that there are two mirrored loops of coolant flow in the machine. Asymmetric circuits are common as well, where there is only one loop and low-temperature fluid is injected on one end. A recent analysis of a ventilation circuit of this type is presented by Ge *et al.* (2022).

The terms *direct cooling* and *indirect cooling* are often encountered when reading about turbo-generators in the power range from 100MVA and up (to more than 2000 MVA). This refers to how the conductors on the rotor and stator sides are cooled. Indirect cooling refers to allowing a coolant flow over the surface of the conductors, outside of the (ground-wall) insulation layer. When direct cooling is employed, cooling channels are embedded in or among the strands of the coils and a coolant is pumped through these channels. These two principles are illustrated in Figure 2.6. The coolant used in indirect cooling is either air (up to 400MVA as presented by Ginet *et al.* (2007)) or hydrogen, which is used for a wide span of powers up to 2000MVA. The direct cooling fluid is either purified water or hydrogen. Information about turbo-generators can be found in the works by Ginet *et al.* (2007); Li *et al.* (2019); Nagakura *et al.* (2009); Han *et al.* (2021). The cooling principles are briefly explained by Stone *et al.* (2014), and are found defined in IEC standard 600034-1:2022 (IEC (2022b))

The intention with these words about cooling arrangements and methods is to highlight that there are several different things that can be considered for deeper studies under the umbrella topic of heat transfer for electric machines. In this thesis the focus will be on machines with indirectly cooled windings, using air as the coolant. In **paper 1** a TEFC-similar traction motor prototype is considered. In **papers 2** and **papers 3** an air jet impinging on a warm surface is studied. In **paper 4** a generic stator slot that can be found in both open and enclosed machines is considered. In **paper 5** heat transfer of an indirectly cooled stator winding is investigated.

2.5. Relative importance of heat transfer coefficient at the end winding of a form wound machine

From a thermal perspective the winding of the machine is a challenge both in design considerations and in analysis. Firstly it needs to carry the currents needed for the energy conversion to take place. This, naturally, gives rise to Joule losses which acts as a volumetric heat source and raises the temperature of the winding. Secondly, the necessary presence of the electrical insulation layer hinders heat dissipation through the low thermal conductivity of such systems (Papkov *et al.* (2007)). Compared to the copper conductor the thermal conductivity of the insulation layer is less than 1/1000th. Thirdly, the insulation system experiences accelerated aging as the temperature increases, which makes

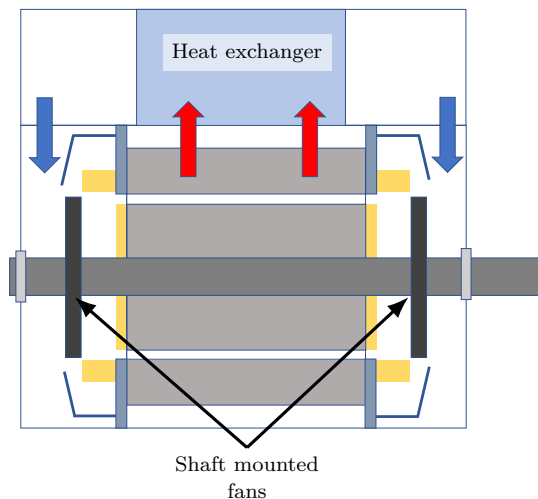


Figure 2.5: Enclosed machine with heat exchanger. In this illustration the cooling is symmetric with two shaft mounted fans. Cool air flows over the active parts to provide cooling, is discharged through the top, where it is cooled with a heat exchanger and returns to complete the circuit.

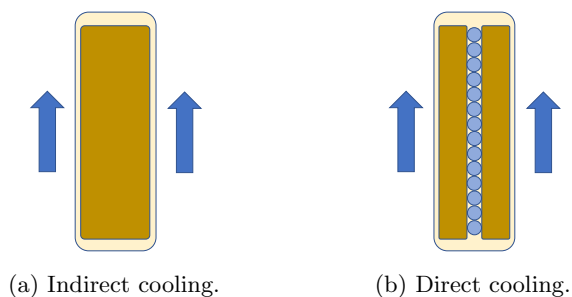


Figure 2.6: Illustration of indirect cooling and direct cooling (combined with indirect) for a 2D cross section of a winding. In indirect cooling the coolant flows over the outside of the winding. In direct cooling coolant channels are embedded in the winding. The illustration for direct cooling is an interpretation based on the image shown by Ginet *et al.* (2007).

it crucial to maintain a permissible operating winding operating temperature for all machine operating conditions.

As the final insulation systems is constituted by different materials, and is realized through a series of manufacturing steps, measured values of the resulting thermal properties are scarce in literature since these would be representative of the specific realization and not be general. Therefore a published value is used as a starting point in the analysis below, and a range of thermal conductivity and thickness of the insulation layer is assumed to illustrate the influence of the insulation layer on the winding's thermal behavior. The quantity used to convey information is the *Biot number* Bergman *et al.* (2017), which is used in relating heat conduction in a solid to the heat transfer at a surface.

The Biot number, a dimensionless quantity, is defined as Bergman *et al.* (2017)

$$Bi = \frac{\eta}{\kappa} L \quad (2.5)$$

where η is the surface heat transfer coefficient, κ is the solid thermal conductivity and L is a characteristic length of the system. The relationship is obtained by taking the ratio of the thermal resistance in the solid $R_{solid} = L/(\kappa \cdot A)$ to the thermal resistance at the fluid-solid interface $R_{interface} = 1/(\eta \cdot A)$. Here, A is a cross sectional area used for computing the respective resistances. The area need to be the same for the two resistances. For non-trivial geometries the parameters L and A need to be estimated or assumed.

The Biot number analysis presented here is performed through approximating the heat flux to be flowing in the horizontal direction, in reference to Fig. 2.7. The conductor width, L_{Cond} , and the insulation thickness, L_{Ins} , are used as characteristic lengths. For the winding the characteristic length is taken as the sum of L_{Cond} and L_{Ins} . The thermal conductivity used for each component is defined by a range. For the conductor characteristic thermal conductivity at $27^\circ C$ of aluminium, $237 \text{ Wm}^{-1} K^{-1}$, and copper, $401 \text{ Wm}^{-1} K^{-1}$, (from CRC Handbook of Chemistry and Physics [John R. Rumble, ed. (2022)]) are used as the limits. For the insulation the value presented by Papkov *et al.* (2007) is used as the nominal value, and the range defined as 70% and 130% of this value. The winding equivalent thermal conductivity is computed from

$$\frac{L_{Cond}}{A \cdot \kappa_{Cond}} + \frac{L_{Ins}}{A \cdot \kappa_{Ins}} = \frac{L_{Eq}}{A \cdot \kappa_{Eq}} \quad (2.6)$$

where $L_{eq} = L_{Cond} + L_{Ins}$. The range limits regarding the winding were established by finding the highest and lowest resistance from the value ranges associated with the conductor and insulator. The values used are given in Table 2.2.

The Biot number for a conductor without the insulation layer, for the insulation layer itself and for a piece of the winding is computed using equation (2.5) for a range of heat transfer coefficients. The computed values are visualized in Fig. 2.8. The ranges for the different components are obtained by forming the extreme values from the values in Table 2.2. Fig. 2.8 shows that if the

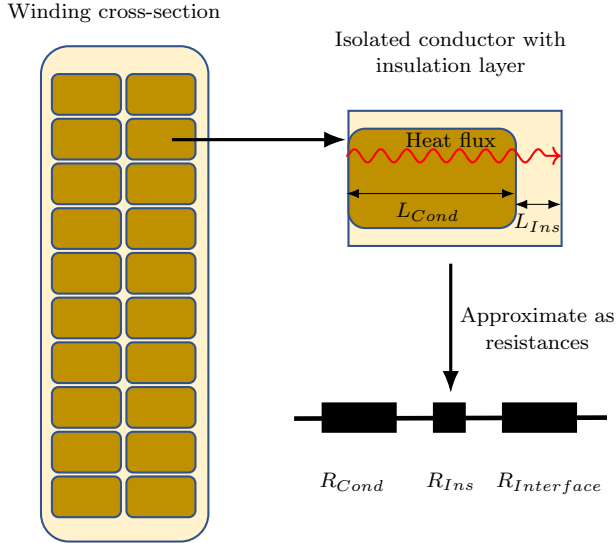


Figure 2.7: Winding cross section simplification for Biot number analysis.

Table 2.2: Thermal conductivity data of winding components

Component	κ (W/(mK))		L (mm)	
	Low	High	Low	High
Conductor	237	401	2.5	10.0
Insulation	0.28	0.42	1.0	2.0
Winding	1.47	1.67	3.5	12.0

conductor is directly exposed to the coolant the rate-controlling phenomena will be the heat transfer to the fluid, through the heat transfer coefficient. This is seen from that the Biot number is much less than 0.1. A Biot number value of $\ll 1$ can be used to indicate whether if the temperature inside the solid can be considered homogeneous or not (Bergman *et al.* (2017)). Due to the low thermal conductivity in the insulation, the heat transfer coefficient will be rate controlling up to around $\eta \approx 40$ while for higher heat transfer coefficients the conduction through the insulation layer becomes limiting. When the Biot number is computed using the winding equivalent values it can be seen that the obtained Biot number range almost perfectly overlaps the ranges associated with the insulation. This illustrates that the electrical insulation defines the heat transfer performance of the winding in the cross-sectional plane.

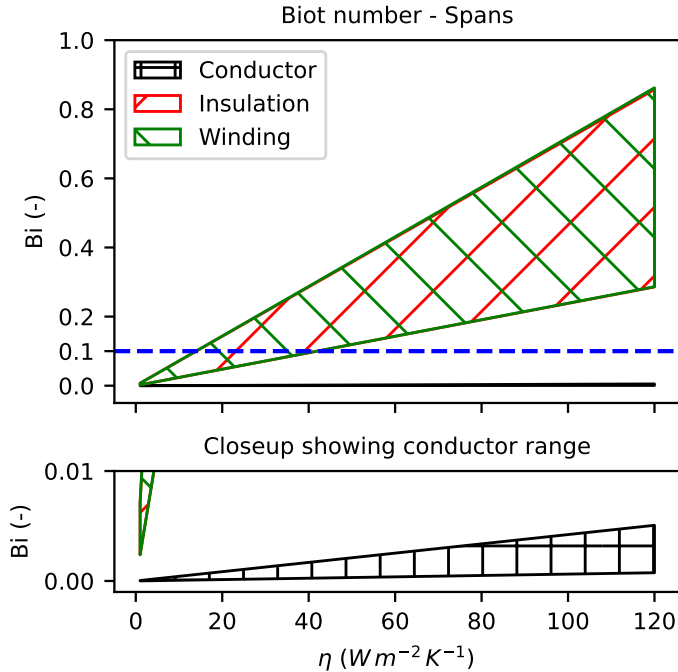


Figure 2.8: Spans of Biot numbers at different heat transfer coefficients h for the conductor, the insulation layer and the isolated conductor (see Fig. 2.7) representing the winding.

The analysis illustrates a few challenges: Since the insulation layer is, in many cases, rate controlling a steep temperature gradient will be found over this part of the winding due to its low thermal conductivity. Due to this temperature gradient the winding temperature need to be measured with sensors that are embedded at the early stages of the manufacturing process, which is commonly done.

Even if the thermal conduction in the insulation layer is rate limiting in many cases, understanding how air is cooling the end winding is of high value. Accurate estimates of the heat transfer coefficient is important since the winding temperature may limit the power density of the machine and dictate which temperature class the insulation need to fulfill, as described in IEC (2007).

2.6. Selected area for research

Given the wide variety of electric machine types, topologies, and cooling methods found in industrial applications, methods for thermal predictions are of high relevance. In many cases performing multiple experiments are challenging, which leads to the question: Can numerical methods be applied for understanding heat transfer on such a detailed level that flow structures causing heat transfer can be understood?

As the electric machine industry has existed for a century now, methods for thermal analysis have been developed and implemented for design and analysis at all major machine suppliers. Continuous enhancement of the predictive capability is essential for designing and delivering high efficiency machines, thus leading to the questions: Which approaches can be applied to improve the predictive capability of thermal analysis tools employed in industry?

Fluid mechanics and heat transfer theory

This chapter describes the equations describing fluid flow and a selection of non-dimensional numbers. The instantaneous incompressible and compressible forms of the equations describing fluid flow are presented, and their averaged versions. For the equations describing the incompressible flows, the Reynolds-averaged versions are stated. In the compressible case the Favere-averaged versions are stated. The presentation draws heavily from the book by Wilcox (2006). In his book the body forces are not included in the equations, which is why they are omitted here as well. The filtered equations used in Large Eddy Simulations (LES) is not described here. For a description of LES, please see e.g. Garnier *et al.* (2009) and the applicable chapters in e.g. Wilcox (2006) and Ferziger (2020).

3.1. Sources of qualitative information

A good source of qualitative information regarding fluid mechanics are the films produced by National Committee for Fluid Mechanics Films (NCFMF (1972)). This is a collection of films, and film notes, that illustrate several topics in the field of fluid mechanics. Another source providing a qualitative introduction to observable fluid dynamics phenomena is found in the book *An album of fluid motion* by Milton Van Dyke (Van Dyke (1982)). In this book 279 photographs of fluid flows, including laminar flows, separation, vortices and more. Both of these sources give refreshing views on the field, showing experiments and how things behave, as an addition to the many equations and theoretical discussions regarding the mathematical descriptions.

3.2. Governing equations - Compressible flow

For a compressible fluid the mass conservation equation reads (see e.g. Wilcox (2006))

$$\frac{\partial \rho}{\partial t} + \frac{\partial}{\partial x_i} (\rho u_i) = 0, \quad (3.1)$$

and the momentum conservation equation, without body forces,

$$\frac{\partial}{\partial t} (\rho u_i) + \frac{\partial}{\partial x_j} (\rho u_j u_i) = \frac{\partial}{\partial x_j} \sigma_{ji}, \quad (3.2)$$

where σ_{ji} is a tensor describing the surface forces acting on the surface of the fluid element. σ_{ji} can be described in terms of pressure forces, p , acting in the normal direction to surfaces, and shear forces, described by the viscous stress tensor t_{ji} , acting across surfaces as

$$\sigma_{ji} = -p\delta_{ji} + t_{ji}. \quad (3.3)$$

Insertion of equation (3.3) into (3.2) gives

$$\frac{\partial}{\partial t}(\rho u_i) + \frac{\partial}{\partial x_j}(\rho u_j u_i) = -\frac{\partial p}{\partial x_i} + \frac{\partial t_{ji}}{\partial x_j}. \quad (3.4)$$

The energy conservation equation, from Wilcox (2006), reads

$$\frac{\partial}{\partial t} \left[\rho \left(e + \frac{1}{2} u_i u_i \right) \right] + \frac{\partial}{\partial x_j} \left[\rho u_j \left(h + \frac{1}{2} u_i u_i \right) \right] = \frac{\partial}{\partial x_j} (u_i t_{ij}) - \frac{\partial q_j}{\partial x_j}, \quad (3.5)$$

in which e is specific internal energy and $h = e + p/\rho$ is specific enthalpy. q_j is heat flux vector. For a gas, the equation of state to use is commonly the ideal gas law

$$p = \rho RT, \quad (3.6)$$

where R is the universal gas constant.

3.2.1. Averaged compressible equations

In order to formulate mean versions of the above equations, the mass averaged velocity \tilde{u}_i is introduced (Wilcox (2006)). The definition of \tilde{u}_i is

$$\tilde{u}_i = \frac{1}{\bar{\rho}} \lim_{T \rightarrow \infty} \frac{1}{T} \int_t^{t+T} \rho(\mathbf{x}, \tau) u_i(\mathbf{x}, \tau) d\tau, \quad (3.7)$$

which gives

$$\bar{\rho} \tilde{u}_i = \overline{\rho u_i}. \quad (3.8)$$

The above allows for writing the Reynolds-averaged continuity equation for a compressible flow (flow with density fluctuations) as

$$\frac{\partial \bar{\rho}}{\partial t} + \frac{\partial}{\partial x_i} (\bar{\rho} \tilde{u}_i) = 0. \quad (3.9)$$

When applying Favre averaging, Wilcox (2006) writes that it is customary to decompose the instantaneous velocity u_i as

$$u_i = \tilde{u}_i + u_i'', \quad (3.10)$$

where \tilde{u}_i is the mass-averaged part and u_i'' is the fluctuating part.

Applying the mass averaging to the momentum, energy equation and ideal gas law gives the Favre averaged mean conservation equations as (Wilcox (2006)) as

$$\frac{\partial \bar{\rho}}{\partial t} + \frac{\partial}{\partial x_i} (\bar{\rho} \tilde{u}_i) = 0. \quad (3.11)$$

$$\frac{\partial}{\partial t} (\bar{\rho} \tilde{u}_i) + \frac{\partial}{\partial x_j} (\bar{\rho} \tilde{u}_j \tilde{u}_i) = -\frac{\partial \bar{P}}{\partial x_i} + \frac{\partial}{\partial x_j} \left[\bar{t}_{ji} - \overline{\rho u_j'' u_i''} \right]. \quad (3.12)$$

$$\begin{aligned}
 \frac{\partial}{\partial t} \left[\bar{\rho} \left(\tilde{e} + \frac{1}{2} \tilde{u}_i \tilde{u}_i \right) + \frac{\overline{\rho u_i'' u_i''}}{2} \right] + \frac{\partial}{\partial x_j} \left[\bar{\rho} \tilde{u}_j \left(\tilde{h} + \frac{1}{2} \tilde{u}_i \tilde{u}_i \right) + \tilde{u}_j \frac{\overline{\rho u_i'' u_i''}}{2} \right] \\
 = \frac{\partial}{\partial x_j} \left[-q_{L_j} - \overline{\rho u_j'' h''} + \overline{t_{ji} u_i''} - \overline{\rho u_j'' \frac{1}{2} u_i'' u_i''} \right] \\
 + \frac{\partial}{\partial x_j} \left[\tilde{u}_i \left(\bar{t}_{ij} - \overline{\rho u_i'' u_j''} \right) \right] \quad (3.13)
 \end{aligned}$$

$$P = \bar{\rho} R \tilde{T} \quad (3.14)$$

Denoting $\frac{\overline{\rho u_i'' u_i''}}{2} = \bar{\rho} k$, where k is turbulence kinetic energy, and the Favre-averaged Reynolds-stress tensor, $-\overline{\rho u_j'' u_i''} = \bar{\rho} \tau_{ij}$, and the turbulent transport of heat $\overline{\rho u_j'' h''} = q_{T_j}$ allows writing the momentum and energy conservation equations as

$$\frac{\partial}{\partial t} (\bar{\rho} \tilde{u}_i) + \frac{\partial}{\partial x_j} (\bar{\rho} \tilde{u}_j \tilde{u}_i) = -\frac{\partial P}{\partial x_i} + \frac{\partial}{\partial x_j} [\bar{t}_{ji} + \bar{\rho} \tau_{ij}] \quad (3.15)$$

$$\begin{aligned}
 \frac{\partial}{\partial t} [\bar{\rho} E] + \frac{\partial}{\partial x_j} [\bar{\rho} \tilde{u}_j H] = \frac{\partial}{\partial x_j} \left[-q_{L_j} - q_{T_j} + \overline{t_{ji} u_i''} - \overline{\rho u_j'' \frac{1}{2} u_i'' u_i''} \right] \\
 + \frac{\partial}{\partial x_j} \left[\tilde{u}_i (\bar{t}_{ij} + \bar{\rho} \tau_{ij}) \right], \quad (3.16)
 \end{aligned}$$

where $E = \tilde{e} + \frac{1}{2} \tilde{u}_i \tilde{u}_i + k$ and $H = \tilde{h} + \frac{1}{2} \tilde{u}_i \tilde{u}_i + k$. Wilcox (2006) derives the averaged compressible turbulence kinetic energy equation to be

$$\begin{aligned}
 \frac{\partial}{\partial t} [\bar{\rho} k] + \frac{\partial}{\partial x_j} [\bar{\rho} \tilde{u}_j k] = \bar{\rho} \tau_{ij} \frac{\partial \tilde{u}_i}{\partial x_j} - \bar{\rho} \epsilon \\
 + \frac{\partial}{\partial x_j} \left[\overline{t_{ji} u_i''} - \overline{\rho u_j'' \frac{1}{2} u_i'' u_i''} - \overline{p' u_j''} \right] - \overline{u_i''} \frac{\partial P}{\partial x_i} + \overline{p' \frac{\partial u_i''}{\partial x_i}}. \quad (3.17)
 \end{aligned}$$

In order to solve the above equations assumptions and models need to be introduced for: shear stresses due to mean flow, \bar{t}_{ij} , Favre-averaged Reynolds stress tensor, $\bar{\rho} \tau_{ij}$, laminar heat flux vector q_{L_j} , turbulent heat flux vector q_{T_j} , turbulence energy dissipation rate $\bar{\rho} \epsilon$, molecular diffusion $\overline{t_{ji} u_i''}$, turbulent transport $\overline{\rho u_j'' \frac{1}{2} u_i'' u_i''}$, pressure diffusion $\overline{p' u_j''}$, pressure dilatation $\overline{p' \frac{\partial u_i''}{\partial x_i}}$, and pressure work $\overline{u_i'' \frac{\partial P}{\partial x_i}}$.

3.2.2. Models and assumptions

The shear stresses need to be modeled differently depending on if the fluid is Newtonian or non-Newtonian¹. For a Newtonian fluid the stress is linearly related to the instantaneous shear rate, and the viscous stress tensor is given by

$$t_{ij} = \mu \left(\frac{\partial u_i}{\partial x_j} + \frac{\partial u_j}{\partial x_i} \right) + \lambda \frac{\partial u_k}{\partial x_k} \delta_{ij} \quad (3.18)$$

¹In the work in this thesis only Newtonian fluids are encountered, why the description is limited to the constitutive relationship for Newtonian fluids.

where μ is the dynamic viscosity and λ is the second coefficient of viscosity. Stokes hypothesis (see e.g. Buresti (2015)) relates μ and λ through the expressions

$$\lambda + \frac{2}{3}\mu = 0, \quad (3.19)$$

which gives $\lambda = -\frac{2}{3}\mu$. Wilcox (2006) writes that this assumption is generally used for all gases in all standard CFD applications, and is correct for a monoatomic gas. After Favre-averaging this reads, after Wilcox (2006),

$$\bar{t}_{ij} = 2\mu\bar{S}_{ij} = 2\mu\left(S_{ij} - \frac{1}{3}\frac{\partial\tilde{u}_k}{\partial x_k}\delta_{ij}\right) = \mu\left(\frac{\partial\tilde{u}_i}{\partial x_j} + \frac{\partial\tilde{u}_j}{\partial x_i}\right) - \frac{2}{3}\mu\frac{\partial\tilde{u}_k}{\partial x_k}\delta_{ij} \quad (3.20)$$

For the Favre-averaged Reynolds stress tensor Wilcox (2006) states that nearly all models are based on the Boussinesq approximation, according to which the principal axes of the Reynolds stress tensor ($\bar{\rho}\tau_{ij}$) are aligned with the mean strain-rate tensor \bar{S}_{ij} , and is assumed to be described by

$$\bar{\rho}\tau_{ij} = 2\mu_T\left(S_{ij} - \frac{1}{3}\frac{\partial\tilde{u}_k}{\partial x_k}\delta_{ij}\right) - \frac{2}{3}\bar{\rho}k\delta_{ij}, \quad (3.21)$$

where μ_T is eddy viscosity.

The instantaneous heat flux vector usually is, according to Wilcox (2006) obtained from Fourier's law of heat conduction as

$$q_j = -\kappa\frac{\partial T}{\partial x_j}. \quad (3.22)$$

If assumed that the fluid is calorically perfect, giving constant specific heat coefficients, the specific internal energy is $e = c_v T$ and specific enthalpy $h = c_p T$. This assumption allows writing the heat flux vector as

$$q_j = -\kappa\frac{\partial T}{\partial x_j} = -\frac{\kappa}{c_p}\frac{\partial h}{\partial x_j} = -\frac{\mu}{Pr_L}\frac{\partial h}{\partial x_j}, \quad (3.23)$$

where $Pr_L = \frac{c_p\mu}{\kappa}$ is the laminar Prandtl number. After Favre-averaging the laminar heat flux vector becomes

$$q_{Lj} = -\frac{\mu}{Pr_L}\frac{\partial\tilde{h}}{\partial x_j} \quad (3.24)$$

Wilcox (2006) writes that the turbulent heat flux vector is commonly assumed to be proportional to the mean temperature gradient as

$$q_{Tj} = -\frac{\mu_T}{Pr_T}\frac{\partial\tilde{h}}{\partial x_j}, \quad (3.25)$$

where the turbulent Prandtl number, Pr_T , is commonly assumed to be 0.89 or 0.90 in a boundary layer, while a value of around 0.5 is more appropriate in free shear layers.

The molecular diffusion and turbulent transport terms are grouped together and, according to Wilcox (2006), commonly approximated as

$$\overline{t_{ji}u_i''} - \overline{\rho u_j'' \frac{1}{2} u_i'' u_i''} = \left(\mu + \frac{\mu_T}{\sigma_k} \right) \frac{\partial k}{\partial x_j}. \quad (3.26)$$

Inserted into the viscous stress tensor gives

$$\tau_{ij} = \mu \left(\frac{\partial u_i}{\partial x_j} + \frac{\partial u_j}{\partial x_i} \right) - \frac{2}{3} \mu \frac{\partial u_k}{\partial x_k} \delta_{ij}. \quad (3.27)$$

Wilcox (2006) writes that little is known about the pressure diffusion, $\overline{p'u_j''}$, and pressure dilatation, $\overline{p' \frac{\partial u_i''}{\partial x_i}}$, that these terms are ignored and implicitly lumped with other terms. Pressure work, $\overline{u_i'' \frac{\partial P}{\partial x_i}}$, may or may not be included depending on the turbulence model employed.

Finally, the turbulence energy dissipation rate $\overline{\rho \epsilon}$ need to be modeled. This model is heavily associated with the turbulence model used. A selection of turbulence models are found described in Wilcox (2006), e.g. the two-equation k- ω and k- ϵ models, where also the effects of compressibility on the turbulence models are discussed. A variant of the k- ω , the k- ω -SST model Menter (1994) with improved wall treatment Menter *et al.* (2003a,b) is used in **paper 5**.

3.3. Governing equations - Incompressible flow

In the notation here, e.g. the instantaneous velocity u_i is decomposed as

$$u_i = \bar{u}_i + u_i', \quad (3.28)$$

where \bar{u}_i denotes the averaged component and u_i' is the fluctuating component.

From Wilcox (2006), the incompressible instantaneous conservation equations from mass and momentum are

$$\frac{\partial u_i}{\partial x_i} = 0 \quad (3.29)$$

$$\rho \frac{\partial u_i}{\partial t} + \rho u_j \frac{\partial u_i}{\partial x_j} = \frac{\partial}{\partial x_j} \sigma_{ji} \quad (3.30)$$

where σ_{ij} is describing surface forces, and as in the compressible equations above given,

$$\sigma_{ji} = -p\delta_{ji} + t_{ji}. \quad (3.31)$$

t_{ji} is the tensor describing the viscous stresses.

3.3.1. Averaged incompressible equations

Performing a suitable type of averaging (volume, time or ensemble) on the equations renders the Reynolds averaged equations as (see Wilcox (2006))

$$\frac{\partial \bar{u}_i}{\partial x_i} = 0 \quad (3.32)$$

$$\rho \frac{\partial \bar{u}_i}{\partial t} + \rho \frac{\partial}{\partial x_j} \left(\bar{u}_j \bar{u}_i + \overline{u'_j u'_i} \right) = -\frac{\partial \bar{p}}{\partial x_i} + \frac{\partial}{\partial x_j} \bar{t}_{ji}, \quad (3.33)$$

where the last equation is often written

$$\rho \frac{\partial \bar{u}_i}{\partial t} + \rho \frac{\partial}{\partial x_j} (\bar{u}_j \bar{u}_i) = -\frac{\partial \bar{p}}{\partial x_i} + \frac{\partial}{\partial x_j} \left(\bar{t}_{ji} - \rho \overline{u'_j u'_i} \right) \quad (3.34)$$

to have the Reynolds stress tensor, $-\rho \overline{u'_j u'_i}$, grouped together with the average molecular stress tensor \bar{t}_{ji} .

The tensor $-\overline{u'_j u'_i}$ is called the specific Reynolds stress tensor (Reynolds stress tensor per unit mass) and is denoted by τ_{ji} . This gives the Reynolds stress tensor as

$$\rho \tau_{ji} = -\rho \overline{u'_j u'_i}, \quad (3.35)$$

and the averaged momentum equation as

$$\rho \frac{\partial \bar{u}_i}{\partial t} + \rho \frac{\partial}{\partial x_j} (\bar{u}_j \bar{u}_i) = -\frac{\partial \bar{p}}{\partial x_i} + \frac{\partial}{\partial x_j} (\bar{t}_{ji} + \rho \tau_{ji}). \quad (3.36)$$

The transport equation for (specific) turbulence kinetic energy is stated by Wilcox (2006) to be

$$\frac{\partial k}{\partial t} + \bar{u}_j \frac{\partial k}{\partial x_j} = \tau_{ij} \frac{\partial \bar{u}_i}{\partial x_j} - \epsilon + \frac{\partial}{\partial x_j} \left[\nu \frac{\partial k}{\partial x_j} - \frac{1}{2} \overline{u'_i u'_i u'_j} - \frac{1}{\rho} \overline{p' u'_j} \right], \quad (3.37)$$

where

$$\epsilon = \nu \overline{\frac{\partial u'_i}{\partial x_k} \frac{\partial u'_i}{\partial x_k}} \quad (3.38)$$

is turbulence kinetic energy dissipation per unit mass. The term $\frac{1}{2} \overline{u'_i u'_i u'_j}$ is called turbulent transport, and the term $\frac{1}{\rho} \overline{p' u'_j}$ pressure diffusion.

3.3.2. Models and assumptions

In an incompressible Newtonian fluid the instantaneous viscous stress tensor is given by

$$t_{ij} = \mu \left(\frac{\partial u_i}{\partial x_j} + \frac{\partial u_j}{\partial x_i} \right), \quad (3.39)$$

where μ is the molecular viscosity. With the instantaneous strain rate tensor s_{ij}

$$s_{ij} = \frac{1}{2} \left(\frac{\partial u_i}{\partial x_j} + \frac{\partial u_j}{\partial x_i} \right) \quad (3.40)$$

the instantaneous viscous stress can be written as

$$t_{ij} = 2\mu s_{ij}. \quad (3.41)$$

Reynolds-averaging gives

$$\bar{t}_{ij} = 2\mu \bar{s}_{ij} = \mu \left(\frac{\partial \bar{u}_i}{\partial x_j} + \frac{\partial \bar{u}_j}{\partial x_i} \right). \quad (3.42)$$

Wilcox (2006) gives a model for the specific Reynolds stress tensor as

$$\tau_{ij} = 2\nu_T \bar{s}_{ij} - \frac{2}{3}k\delta_{ij}, \quad (3.43)$$

which is based on that the Boussinesq assumption is valid, according to which the principal axes of the Reynolds stress tensor ($\rho\tau_{ij}$) are aligned with the mean strain-rate tensor \bar{s}_{ij} . In the above expression ν_T is turbulent dynamic viscosity, which need approximation.

The turbulent transport and pressure diffusion terms are, as stated by Wilcox (2006), treated together as

$$\frac{1}{2}\overline{u'_i u'_i u'_j} + \frac{1}{\rho}\overline{p' u'_j} = -\frac{\nu_T}{\sigma_k} \frac{\partial k}{\partial x_j}, \quad (3.44)$$

where σ_k is a closure coefficient. Combined together, the above equations form the turbulence kinetic energy equation commonly found in turbulence models (Wilcox (2006)) as

$$\frac{\partial k}{\partial t} + \bar{u}_j \frac{\partial k}{\partial x_j} = \tau_{ij} \frac{\partial \bar{u}_i}{\partial x_j} - \epsilon + \frac{\partial}{\partial x_j} \left[\left(\nu + \frac{\nu_T}{\sigma_k} \right) \frac{\partial k}{\partial x_j} \right]. \quad (3.45)$$

As mentioned in the description of the compressible equations above, a selection of turbulence models are found described in Wilcox (2006).

3.4. Dimensionless numbers

Dimensionless numbers are useful in that they can describe similarities between systems of different dimensions. The similarity concept allows for conclusion drawn from one study can be applied to another system as long as they both are described by the same dimensionless quantities.

The original source where Edgar Buckingham presented what is now referred to as the **Buckingham Pi theorem** appear to be Buckingham (1914). The Buckingham Pi theorem states that from n dimensional variables of k fundamental dimensions, $p = n - k$ dimensionless parameters can be constructed from the original variables.

The **Reynolds number** (Re) combines geometrical dimension (l) with velocity (u), viscosity (μ) and density (ρ) as

$$Re = \frac{\rho ul}{\mu} = \frac{ul}{\nu}. \quad (3.46)$$

Here, ν is the kinematic viscosity $\nu = \mu/\rho$. The Reynolds number is often use to classify the flow as non-turbulent or turbulent. For this characterization, using the Reynolds number, the bodies from which the length scale is obtained should be geometrically similar. The geometric similarity means that one shape can be obtained from another by changing all linear dimensions by the same scaling parameter (Landau & Lifshitz (1987)).

In non-steady flows, i.e. flows with oscillations, the Strouhal number provides a dimensionless frequency characteristic. The **Strouhal number**

(Sr) relates a characteristic frequency (f) with flow velocity and a geometric dimension,

$$Sr = \frac{lf}{u}. \quad (3.47)$$

Two systems with the same Reynolds number and Strouhal number exhibit similar dynamic motion (Landau & Lifshitz (1987)).

The **Mach number** (Ma) relates the speed of sound in the fluid to the velocity of the flow considered. The Mach number is expressed as

$$Ma = \frac{u}{c}, \quad (3.48)$$

where u is the flow velocity and c is the speed of sound in the fluid under consideration. When $Ma < 0.3$ the flow can be treated as incompressible (Ferziger (2002)).

The **Knudsen number** is relating the mean free path λ with a geometric dimension l . The mean free path is *the average path a molecule travels between two consecutive collisions*. The Knudsen number is written as

$$Kn = \frac{\lambda}{l}. \quad (3.49)$$

by Kandlikar *et al.* (2014). When $Kn > 10^{-1}$ the continuum approach is not valid and the Navier-Stokes equations cannot be used. For $10^{-3} < Kn < 10^{-1}$ Navier-Stokes equations are valid but special velocity and slip conditions at wall need to be applied. When $Kn < 10^{-3}$ the continuum approximation is fully valid and the N-S equations with no-slip wall boundary conditions can be used (Kandlikar *et al.* (2014)).

The **Stokes number** relates the characteristic time of a particle with the characteristic time of the flow. In Krstic (2006) it is explained as *The Stokes number is the ratio of the particle's momentum response time to the flow-field time scale*. The stokes number can be expressed as

$$Stk = \frac{t_0}{l/u}, \quad (3.50)$$

where t_0 is the *relaxation time of the suspended particle*, l is a characteristic length of the flow geometry and u is a characteristic speed.

A large Stokes number ($Stk \gg 1$) means that particles transported by the fluid will be prone to detach from the flow, when it is close to unity ($Stk \approx 1$) the particles will follow the flow, and when it is much less than unity ($Stk \ll 1$) particles will follow the flow very closely.

The Stokes number can be used when performing particle image velocimetry (PIV) experiments to judge how well the injected particles will represent the flow field. The lower the Stokes number, the better representation.

In describing thermal properties of a fluid the non-dimensional **Prandtl number** (Pr) is used. This non-dimensional quantity relates the viscosity of

the fluid with the thermal diffusivity as

$$Pr = \frac{\nu}{\alpha} = \frac{\mu/\rho}{\kappa/(\rho c_p)} = \frac{\mu c_p}{\kappa}. \quad (3.51)$$

In this context κ is the thermal conductivity of the fluid and α denotes the thermal diffusivity, $\alpha = \kappa/(\rho c_p)$. Flows described by the same Reynolds number and Prandtl number are similar (Landau & Lifshitz (1987)). In Versteeg (2007) this is described as the ratio of *rate of momentum transport* to *rate of energy transport*.

The **Schmidt number** relates the *rate of momentum transport* to *rate of mass transport* (Versteeg (2007)) as

$$Sc = \frac{\nu}{D} = \frac{\mu/\rho}{D}, \quad (3.52)$$

where D is the diffusion coefficient.

The **Peclet number** relates the strengths of advection and diffusion (Versteeg (2007)). Depending on the quantity under investigation, a thermal or mass transfer Peclet number can be defined. For mass transfer it is

$$Pe = \frac{lu}{D} = Re_l Sc, \quad (3.53)$$

and for heat transfer it is

$$Pe = \frac{lu}{\alpha} = Re_l Pr, \quad (3.54)$$

where l is a characteristic length of the system, u a characteristic speed, Sc is the Schmidt number and Pr is the Prandtl number. The Peclet number can hence be obtained as a multiple between the Reynolds number and Schmidt or Prandtl number depending on which quantity is of interest. When the Peclet number tends to zero ($Pe \rightarrow 0$) the transport is diffusion dominant, and when it tends to infinity it is convection dominant ($Pe \rightarrow \infty$) (Versteeg (2007)).

The **Lewis number** relates the diffusivity of a species with the thermal diffusivity. If D_k denotes the diffusivity of species k , the Lewis number for the species can be written as (Poinso (2001); Versteeg (2007))

$$Le_k = \frac{\alpha}{D_k} = \frac{\kappa}{\rho c_p D_k}. \quad (3.55)$$

where α is the thermal diffusivity, c_p is the specific heat capacity and ρ the fluid density. The Lewis number can also be expressed with a mixture-averaged diffusion coefficient (D) to obtain a Lewis number for the mixed fluid.

When heat transfer occurs between a solid body and a fluid it is common to describe this using a heat transfer coefficient, η . A non-dimensional number relating the heat transfer coefficient, h , with a characteristic length and fluid thermal conductivity is the **Nusselt number** (Nu). This is expressed as

$$Nu = \frac{l_{fluid}/\kappa_{fluid}}{1/\eta} = \frac{h \cdot l_{fluid}}{\kappa_{fluid}}. \quad (3.56)$$

The **Biot number** is useful for finding which heat transfer mechanism is limiting when investigating heat transfer between solid bodies and fluids (Bergman *et al.* (2017); Lienhard & Lienhard (2020); VDI Gesellschaft (2010)), and can be interpreted as the ratio of two series resistances (VDI Gesellschaft (2010)). It can be expressed as

$$Bi = \frac{l_{solid}/\kappa_{solid}}{1/\eta} = \frac{\eta \cdot l_{solid}}{\kappa_{solid}}, \quad (3.57)$$

where l is a characteristic length of the heat transfer path in the solid (e.g. the diameter of a particle), κ_{solid} is the thermal conductivity of the solid, and η is the heat transfer coefficient between the solid and the fluid. If the Biot number is larger than unity, then the thermal resistance in the solid is dominating. Conversely, if it is smaller than unity then the heat transfer from the solid to the fluid constitutes the main resistance in the heat transfer.

Methods

This chapter gives a brief introduction of numerical methods employed in thermal analysis of electric machines. The Lumped Parameter Thermal Network (LPTN) method and Finite Volume Method (FVM) are mentioned. In relation to Model Order Reduction (MOR) the Proper Orthogonal Decomposition (POD) and Extended POD is recapitulated from Rönnerberg (2020).

4.1. Thermal and fluid flow simulations

The Lumped Parameter Thermal Network (also called Thermal Equivalent Network) model is a method commonly employed for thermal analysis of electrical equipment such as motors. Its popularity in electrical engineering can likely be due to the analogies between electrical and thermal quantities and behavior. Finite Element Analysis (FEA) is also a common method employed in analysis of temperature fields and heat transfer in the electric machine domain. While FEA can be employed in fluid dynamics analysis, described e.g. in the book by Zienkiewicz (2014), in the (rotating) electric machine domain FEA typically considers temperature and heat transfer in the solids of the machine. Heat transfer to fluids are considered through boundary conditions based on correlations, such as those found in the book from VDI Gesellschaft (2010), in both the LPTN and FEA approaches in machine design. Computational Fluid Dynamics (CFD) has been in use in electric machine analysis, and has recently been employed to resolve large parts of the cooling circuit as in the work by Ge *et al.* (2022). Both the finite element method and the finite volume method are methods for discretizing partial differential equations for numerical solution. A comprehensive introduction to methods for numerical solution of differential equations, focusing on the finite element method but also covering finite volume, finite differences, and spectral methods, can be found in the book by Quarteroni (2017).

A book that covers several aspects of rotating electric machine cooling methods and thermal analysis, is the book by Staton *et al.* (2022). Here the emphasis is on the LPTN method, but FEA and CFD is also covered. The lumped parameter thermal networks are sometimes referred to as thermal equivalent circuits. Pyrhonen *et al.* (2014) have a section dedicated to the thermal equivalent circuit, which is a good introduction to the topic. A section

on the thermal equivalent circuit can also be found in the book by Lipo (2017). The analogy between thermal and electrical quantities presented by Pyrhonen *et al.* (2014) is shown in Table 4.1.

Table 4.1: Analogies between thermal flow and electrical flow quantities. Information is retrieved from Pyrhonen *et al.* (2014).

Thermal flow	Unit	Electric flow	Unit
Quantity of heat	J	Electric charge	C
Heat flow rate	W	Electric current	A
Heat flow density	W/m ²	Current density	A/m ²
Temperature	K	Electric potential	V
Temperature rise	K	Voltage	V
Thermal conductivity	W/(m K)	Electric conductivity	S/m = A/(V m)
Thermal resistance	K/W	Electric resistance	$\Omega = V/A$
Thermal conductance	W/K	Electric conductance	S = A/V
Heat capacity	J/K	Capacitance	F = C/V

To illustrate a simple steady state LPTN discretization, the cross section of the winding strand illustrated in Fig. 2.7 can be used. Isolating the strand and introducing nodes at the leftmost and rightmost side of the copper conductor, at the insulation interface to the fluid and in the fluid stream, it can be graphically illustrated as in Fig. 4.1. The winding strand is thus assigned four nodes according to the selection above. The selection can be made differently. Here the loss generated in the piece of the winding considered is P_{Cond} , and is assigned to the innermost node (node 1). The resistances are approximated as $R_{Cond} = L_{Cond}/(A_{Cond} \cdot \kappa_{Cond})$, $R_{Ins} = L_{Ins}/(A_{Ins} \cdot \kappa_{Ins})$ and $R_{Interface} = 1/(\eta_{Interface} \cdot A_{Interface})$. The node temperatures can now be found by computing $(T_i - T_{i+1}) = R_i \cdot q_i$, which can be assembled into a matrix system and computed using matrix solver techniques.

The advantage of this method is that it is computationally fast, while a drawback is that it requires input in the form of heat transfer correlations to describe the heat transfer coefficients, h , occurring in the equations. As the heat transfer coefficient is dependent on system properties, dedicated investigations are needed to establish these correlations for the system considered. In **paper 5** a CFD study is employed to arrive at a description of the heat transfer coefficient at the end winding region of a machine, which can be used in LPTN definitions. In **paper 4** the LPTN method is used for simulating a half-tooth-half-slot geometry of a generic stator. Here the electrical analogy of the thermal network was exploited and the system was solved using the circuit simulator PySpice (Salvaire (2021)).

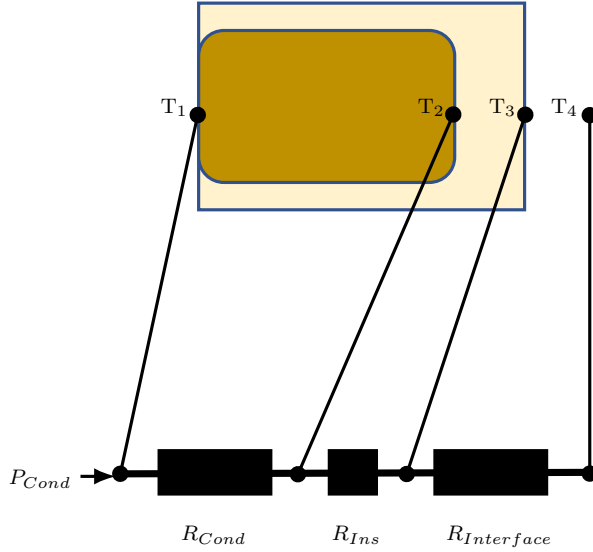


Figure 4.1: Steady state lumped parameter thermal network for the isolated conductor from Fig. 2.7. T denotes temperature, P loss (power), and R thermal resistance.

The Finite Volume Method (FVM) is a discretization method extensively used in fluid flow simulations. There are several books on the topic of computational fluid dynamics using the finite volume method. Two examples are the book by Ferziger (2020) and the book by Versteeg (2007). An advantage of the FVM is that the control volumes used in the discretization can accommodate any type of grid, and therefore it is applicable for complex geometries (Ferziger (2020)).

The FVM is based on formulating the integral form of the equations that are to be solved, and performing the integrations over discrete and finite control volumes. This can be exemplified considering the instantaneous incompressible continuity equation, eq. (3.29), and momentum equations, eq. (3.30), for a Newtonian fluid, which has viscous forces described by eq. (3.39). Using equations eq. (3.31) and eq. (3.39), combined with the incompressible continuity eq. (3.29), and division by the constant ρ , gives the Navier-Stokes equation for an incompressible flow as

$$\frac{\partial u_i}{\partial x_i} = 0 \quad (4.1)$$

$$\frac{\partial u_i}{\partial t} + u_j \frac{\partial u_i}{\partial x_j} = -\frac{\partial}{\partial x_i} \left(\frac{p}{\rho} \right) + \nu \frac{\partial^2 u_i}{\partial x_j \partial x_j}, \quad (4.2)$$

where $\nu = \mu/\rho$ is the kinematic viscosity. Re-arrangement and utilization of the continuity equation allows for re-writing eq. (4.2) as

$$\frac{\partial u_i}{\partial t} = \frac{\partial}{\partial x_j} \left(-u_j u_i - \frac{p}{\rho} \delta_{ij} + \nu \frac{\partial u_i}{\partial x_j} \right). \quad (4.3)$$

Integration of this equation over a fixed control volume element with volume V_c gives

$$\begin{aligned} \int_{V_c} \frac{\partial u_i}{\partial t} dV &= \frac{\partial}{\partial t} \int_{V_c} u_i dV \\ &= \int_{V_c} \left[\frac{\partial}{\partial x_j} \left(-u_j u_i - \frac{p}{\rho} \delta_{ij} + \nu \frac{\partial u_i}{\partial x_j} \right) \right] dV \\ &= \int_{\partial V_c} \left(-u_j u_i - \frac{p}{\rho} \delta_{ij} + \nu \frac{\partial u_i}{\partial x_j} \right) n_j dS, \end{aligned} \quad (4.4)$$

where the first step, commutation of integration and differentiation with time, is achieved through the use of a fixed control volume, and the last step, transformation from a volume integral to a surface integral is achieved using Gauss' theorem. Here, ∂V_c denotes the closed surface of the control volume considered, and n_j is the outward-pointing surface normal. Applying integration over control volume to the continuity equation gives

$$0 = \int_{V_c} \frac{\partial u_i}{\partial x_i} dV = \int_{\partial V_c} u_i n_i dS. \quad (4.5)$$

For solving the equations over a domain of interest, the domain need to be discretized in order to define control volumes of suitable sizes. This step is what is commonly referred to as *meshing*. The mesh need to be defined to resolve the physics and phenomena of interest. Both Ferziger (2020) and Versteeg (2007) have chapters discussing structured and unstructured meshes, and what to consider for complex geometries. Once the discretization of the domain is in place, approximations of the equations of interest can be introduced. For a complete description suitable literature, such as Ferziger (2020) and Versteeg (2007), is to be consulted. Together with boundary conditions the approximation of the discretized equations are assembled into an algebraic equation system that can be solved using different equation solvers and, for unsteady problems, time integration methods. Additionally, calculation strategies for in which order and how to solve for momentum, pressure, scalars, and fluid properties. Examples of such methods are fractional step methods, the Semi-Implicit Method for Pressure-Linked Equations (SIMPLE) algorithm and its variants (SIMPLER, SIMPLEC), and Pressure Implicit with Splitting of Operators (PISO). For introductions to these methods, specialized literature such as, again, Ferziger (2020) and Versteeg (2007) is best referred to.

There exist both commercial and open source toolkits for meshing and fluid dynamics simulations built around the finite volume method. In **paper 1**

a commercial meshing solution, and commercial CFD simulation tool (CFX) was employed. In **paper 2**, **paper 3** and **paper 5** the open source toolkit OpenFOAM (Weller *et al.* (1998)) is used.

4.2. Model order reduction

Model Order Reduction (MOR) is based on capturing the dominant behavior of a system with as small a description as sufficient. Two high-level classifications of MOR is described in Benner *et al.* (2021): system theory based, and numerical analysis solutions based. In the system-theoretic approaches the starting point are the set of Ordinary Differential Equations (ODE) or Differential Algebraic Equations (DAE) describing the system of consideration, and the objective is to find a smaller set of equations that approximates the system response to a sufficient level. In the numerical analysis solution based approach, partial differential equations (PDE) are discretized and solved numerically. The field data obtained is sampled, and methods are applied on the sampled set to obtain a reduced order representation that approximates the behavior of the exact solution. Sometimes the words *sample* and *snapshot* are used interchangeably. Several MOR techniques, both system-theoretic and numerical analysis based, are found describe in the three volume collection on Model Order Reduction by Benner *et al.* (2021, 2020a,b).

In the work presented in this thesis (**paper 3**) methods belonging to the numerical analysis solution based approach, namely POD and the Extended Proper Orthogonal Decomposition (EPOD) were employed. EPOD is not covered in the works by Benner *et al.* (2021, 2020a,b). The EPOD method allows for correlating two physical quantities, and was introduced in the work by Borée (2003). The POD and EPOD methods were described in Rönnerberg (2020), and only a recapitulation will be given here.

A scalar field, $A(x, y, z, t)$, or vector field, $\mathbf{A}(x, y, z, t)$, can with the POD method be decomposed as

$$i = 1, \dots, n_c \quad A_i(x, y, z, t) = \sum_n a(t)^{(n)} \Phi_i^{(n)}(x, y, z), \quad (4.6)$$

where n_c is the number of components in the considered field, n is the *mode order*, $a(t)^{(n)}$ are the time dependent coefficients associated with each mode, and $\Phi_i^{(n)}(x, y, z)$ are the spatial basis functions. The time coefficients $a(t)^{(n)}$ are found by projecting each discrete snapshot of the physical process on the spatial basis functions through

$$a(t_k)^{(n)} = \langle \langle A_i(\mathbf{x}, t_k), \Phi_i^{(n)}(\mathbf{x}) \rangle \rangle, \quad (4.7)$$

where $\langle \langle \cdot, \cdot \rangle \rangle$ denotes a suitable inner product. With M time samples (snapshots), this will render $[a(t_1)^{(n)}, \dots, a(t_M)^{(n)}]$. The mode coefficients $a(t)^{(n)}$ and the eigenvalues of the decomposition (see e.g. Rönnerberg (2020)) are related through

$$\frac{1}{M} \sum_k \left(a(t_k)^{(n)} \right)^2 = \lambda^{(n)}. \quad (4.8)$$

The eigenvalues can be interpreted as the respective modes' contribution to the overall variance of the considered quantity. If the decomposed field is the velocity field, the eigenvalues are often referred to as *kinetic energy*. In the Extended POD, the mode coefficients and eigenvalues obtained from the POD decomposition are used to associate quantity $A(x, y, z, t)$ with $B(x', y', z', t)$, through

$$\Psi^{(p)}(\mathbf{x}') = \frac{\langle a^{(p)}(t)B(\mathbf{x}', t) \rangle}{\lambda^{(p)}}, \quad (4.9)$$

where, $\langle \cdot \rangle$ is an averaging operator. Here $a^{(p)}(t)$ are the mode coefficients for mode p established through POD and $\lambda^{(p)}$ is the corresponding eigenvalue for mode p , and the result $\Psi^{(p)}(\mathbf{x}')$ is the extended mode basis function.

MOR is typically employed with the intention to use the reduced order model to simulate or predict the original process. This was not the end goal in the study presented here. Instead, in **paper 3**, the individual spatial modes of the POD and EPOD decomposition were analyzed for visualizing the spatial structures associated with the modes. The normalized eigen value spectrum was analyzed and showed that the dominating modes were of low relative strength, meaning that reconstruction of the governing system would require many modes.

Investigations

This chapter discusses considerations to be taken when defining and comparing simulation data to lab measurements (paper 1), how numerical methods can be used for introducing new cooling features in electric machines (papers 2 and 3), and how numerical methods can be used in supporting development of design and analysis tools for electric machines (papers 4 and 5).

5.1. Considerations for temperature measurements on lab scale setups (Paper 1)

As Moses *et al.* (2019b) reflects on, a true temperature level measurement in a rotating electrical machine need to be performed with a load. When the machines are modestly sized it is possible to arrange a setup where one machine acts as a load, operating in generative mode, and one machine operates in motoring mode. Depending on which machine is the test object depends on what operating characteristics is of interest. For a motor the test object is operating in motoring mode. An example on the use of a setup with motor and load can be found in Fasil *et al.* (2014), where a hub motor is tested under load using a gearbox and generator on the load side.

An illustration of the principles of a back-to-back setup is shown in Figure 5.1. The illustration shows two machines, connected mechanically through their shafts, with a torque meter mounted at the coupling joint. Both machines, which in the illustration are 3-phase machines, are connected to one converter each. What is commonly measured in back-to-back measurements are the input voltage and current to the motor, the mechanical power transferred between the machines, and temperature.

The advantage with a back-to-back setup with both machines controlled by converters is that different operating points (torque & speed combinations) can be achieved. For machines for industrial purposes the machine design is typically optimized for continuous operation. This is designated as the S1 duty cycle (continuous running duty) according to IEC standard 600034-1:2002 (IEC (2022b)). This type of duty is also used in other applications, such as traction applications, during design evaluation. As continuous operation is of main interest, the steady-state temperature levels are also of main interest. During measurements, thermal equilibrium is reached when several parts of the

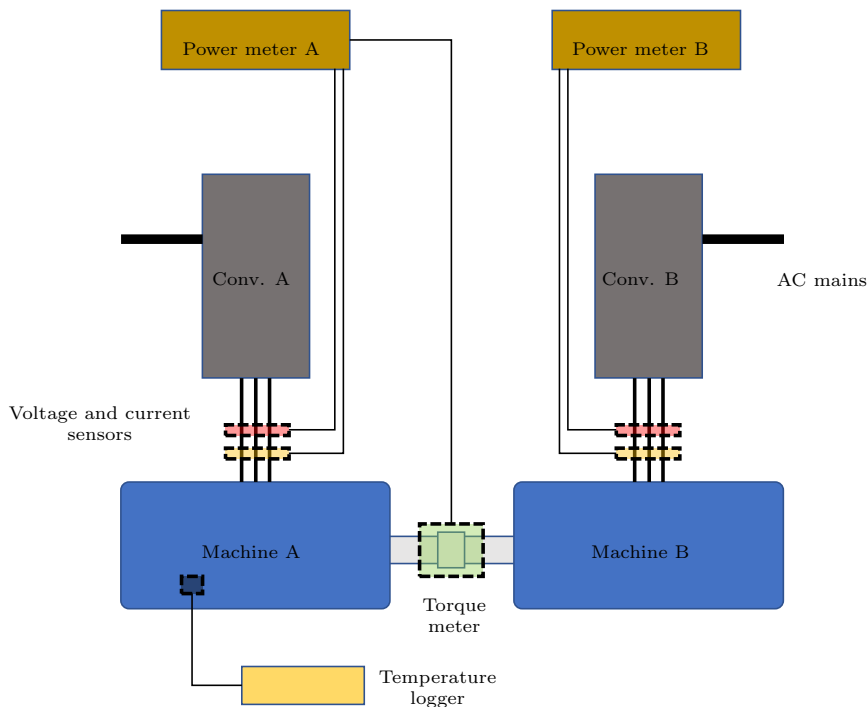


Figure 5.1: Principle sketch of a back-to-back setup. Both machines are connected to converters. The sketch shows two AC drives with separate mains.

machine does not vary by more than 1K per half-hour as defined in standard IEC 600034-1:2022 (IEC (2022*b*)). Temperature measurements of windings can be realized through two approaches: with temperature sensors and through winding resistance. With the resistance method the temperature of the winding is related to the electrical resistivity of the winding. The advantage with the resistance method is that the average temperature of the winding is obtained in one measurement, the disadvantage is that it typically cannot be performed during operation as the supply need to be disconnected and the resistance measured. With temperature sensors it is possible to perform continuous measurements, while the drawback is that only local measurements are possible. I.e. it is only possible to obtain temperature information from where the sensor is mounted. During prototype and experimental testing it is possible to equip a machine with several temperature sensors. Standard IEC 600034-1:2022 (IEC (2022*b*)) distinguishes between three methods of measurement of temperature: resistance method, embedded temperature detector (ETD) method, and thermometer method. The difference between the ETD method and thermometer method is mainly when during the manufacturing process the sensors are introduced.

ETD:s are introduced at points of the machine which are inaccessible after assembly is complete, while thermometers can be introduced or mounted at accessible surfaces of the completed machine. An illustration of where ETD:s and thermometers may be located is found in Figure 5.2.

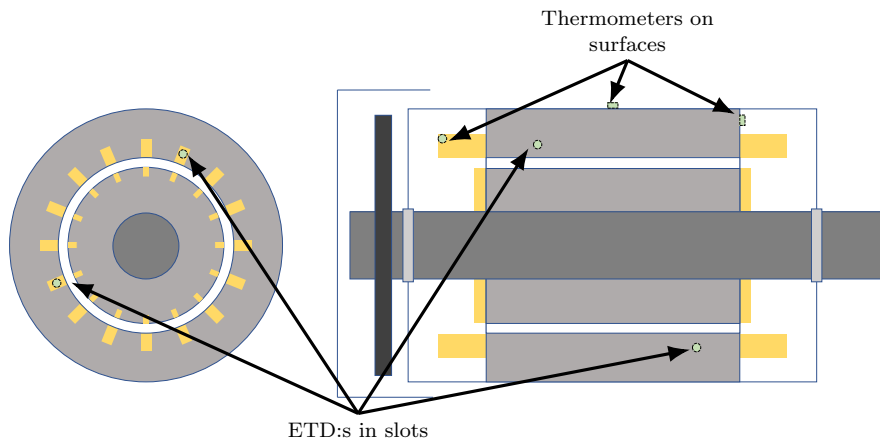


Figure 5.2: Illustrations of embedded temperature detectors (ETD) and thermometers. While the devices may be the same, installation during manufacturing or after differs according to standard IEC 600034-1:2002 (IEC (2022b))

Thermal model and simulation approach development for electrical machines is in many cases accompanied by experiments, when possible of the back-to-back type discussed above. For evaluation of model performance computed temperature values are compared to measured values. Depending on the symmetry of the machine, simulation assumptions affect the outcome of the comparison. In **paper 1** simulation assumptions related to loss distribution and air flow distribution in the axial cooling channels of a traction motor prototype are explored and related to measured values. What was investigated was if a spatial loss distribution compared to a homogeneous loss distribution, combined with an evenly or un-evenly distributed flow through the axial channels would affect the simulated temperature enough to influence the comparison with measured values. What was observed was that, for this machine and test, adjustments of the simulation assumptions altered the simulated temperature profile in the machine. The changes in simulated temperature distribution indicate that the placement of ETD:s could be considered when preparing a machine for experiments, in order to capture local temperature maxima during measurements.

5.2. Computational methods to use for introducing new cooling features (Papers 2 & 3)

It is desirable in the product development to make as accurate predictions of design modifications as possible at the analysis stage, before moving into prototyping and testing. In many cases it is desirable to utilize established design tools and approaches to assess the influence on the system of a modification. Thermal analysis routines of electric machine design tools are often based on an analytical description of the machine in the form of an equivalent circuit. This approach is often referred to as Thermal Equivalent Circuit (Lipo (2017); Pyrhonen *et al.* (2014)) or Lumped Parameter Thermal Network (LPTN) (Mellor *et al.* (1991); Staton *et al.* (2022)). This approach, which is often computationally fast, relies on correlations for describing heat transfer between fluid and solid regions.

Access to correlations describing heat transfer phenomena is therefore crucial for making machine-level assessments of introduction of new cooling features. An extensive range of correlations and information can be found compiled in VDI Gesellschaft (2010), which can be implemented in LPTN studies. In applying correlations it is necessary to consider whether the condition the correlation was established under is similar to the conditions that will be experienced in the application under consideration. When additional information is needed, Computational Fluid Dynamics (CFD) studies can be employed to understand the heat transfer mechanisms underlying to the correlation and to establish new correlations.

In **paper 2** and **paper 3** heat transfer from a round jet impinging on a flat plate is studied using Large Eddy Simulation (LES) type CFD simulation. The simulations resolved both temporal and spatial phenomena. The time-resolved data was averaged in order to generate a spatial correlation showing heat transfer as a function of radial distance to the impingement center. For investigating the link between structures in the flow and heat transfer Extended Proper Orthogonal Decomposition was employed. Understanding this link may allow for identification of structures associated with high heat transfer. Further investigation could then be directed towards understanding if the occurrence of such structures could be increased through modifications to system parameters or geometry. It is possible to anticipate that similar studies, dedicated to machine-related features, could be employed to gain a deeper understanding of heat transfer phenomena in machines. Additionally, it is possible to anticipate that similar studies can be employed to study and understand new cooling systems, new cooling features, and potential for enhancement of existing heat flow paths.

5.3. New features for design tools (Papers 4 & 5)

Design tools for electric machines need to balance computational speed and accuracy. For thermal analysis this can be achieved by combining methods tailored for different purposes. The Lumped Parameter Thermal Network

(LPTN) / Thermal Equivalent Circuit is a method used extensively in numerical thermal studies of electrical machines during design. An early description of the use of a LPTN for motor studies was given by Mellor *et al.* (1991). Due to its popularity it is covered in books such as those by Lipo (2017) and Pyrhonen *et al.* (2014), and Staton *et al.* (2022), and is used, improved and extended in works by e.g. Ghahfarokhi *et al.* (2020), Madonna *et al.* (2019) and Liang *et al.* (2021). The LPTN is computationally fast and shows good predictive performance when coupled with suitable heat transfer correlations and subjected to proper calibration.

Staton *et al.* (2022) explains that model calibration is necessary to increase the accuracy of the predictions. The need for calibration is due to that there are manufacturing uncertainties that have an influence on the machine temperature rise. Some examples, which are directly relatable to low voltage industrial motors, are presented in Staton *et al.* (2022). A rephrased selection of some of these are:

- Thermal contact interface between stator and housing.
- Contact interface between winding and stator.
- Impregnation penetration in winding.
- External cooling performance for TEFC machines.

An illustration showing where these uncertainties occur is shown in Figure 5.3. The above listed uncertainties are not well known at the design stage. This is especially true when dealing with machine development projects and new prototypes. Examples on the performance of a-priori defined, un-calibrated, thermal models compared to calibrated models are presented by Boglietti *et al.* (2019). In the same paper methods to perform experiments to collect measurement data for calibration are also presented and explained.

It is desirable to find an automated approach for updating a LPTN definition based on temperature inputs collected during machine tests. A prototype of such an approach is described in **paper 4**. Here an application of machine learning (ML) methods are reported for adjustment of a LPTN model of a stator half-slot-half-tooth geometry. The thermal network is implemented as a SPICE (Simulation Program with Integrated Circuit Emphasis) netlist (Nagel & Pederson (1973)) and solved using PySpice version 1.4.3 (Salvaire (2021)). For defining the training database needed for the ML methods, it is built using variations to a base network. Machine learning models are then trained on this database, and their prediction capability tested using perturbations to the base network. The machine learning framework used was Scikit-learn version 0.23.1 (Pedregosa *et al.* (2011)). The approach shows promising results in the assessments made, and further investigations are of interest.

Introduction of new correlations in LPTN tools are sometimes needed. CFD can be used for specific investigations and to derive relationships that can be implemented in design tools. In **paper 5** a CFD study is performed for the end-winding region of a form-wound low-speed induction machine where forced cooling can be supplied from an external cooling system. Based on

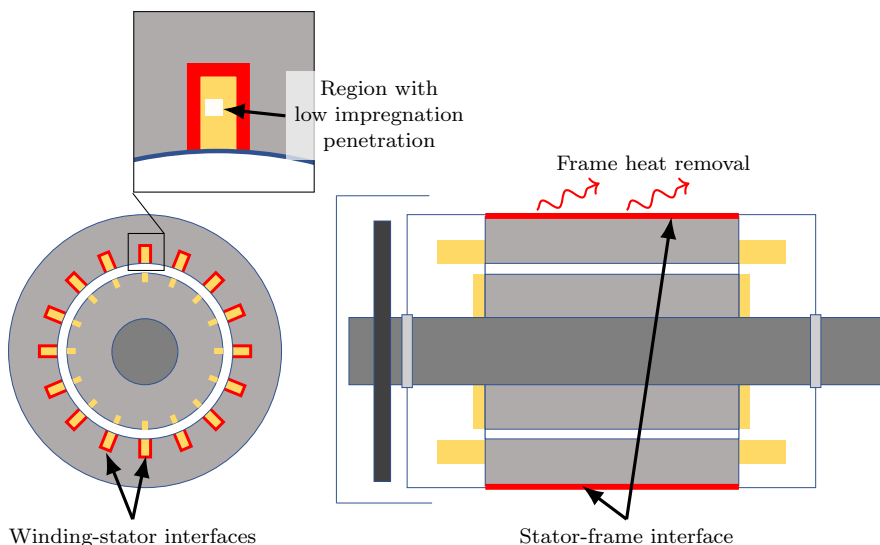


Figure 5.3: Illustrations of selected uncertainties mentioned by Staton *et al.* (2022).

the simulation data, a correlation describing the surface-average heat transfer coefficient, $\bar{\eta}$, at the end winding as a function of rotor surface speed, v_s , and inlet flow speed, v_{in} , is obtained. The correlation proposed is on the form

$$\bar{\eta}(v_{in}, v_s) = a \cdot v_{in}^b + c \cdot \exp(-v_{in} \cdot d) \cdot v_s^e + f, \quad (5.1)$$

where a , b , c , d , e , and f are fitted to simulation data. A well-established correlation for purely rotor-driven flows is

$$\bar{\eta}(v) = k_1 \left(1 + k_2 \cdot v^{k_3} \right), \quad (5.2)$$

and is used by e.g. Boglietti *et al.* (2009); Mellor *et al.* (1991); Gilson *et al.* (2009) and Boglietti & Cavagnino (2007). When $v_{in} = 0$ equation (5.1) reduces to equation (5.2)

$$\begin{aligned} \bar{\eta}(v_{in} = 0, v_s) = c \cdot v_s^e + f &= \left\{ f = k_1, \quad \frac{c}{f} = k_2, \quad e = k_3 \right\} \\ &= k_1 \left(1 + k_2 \cdot v_s^{k_3} \right), \end{aligned} \quad (5.3)$$

indicating that the correlation can be used for both purely rotor-driven flow and when external cooling is supplied. The proposed correlation was implemented in an in-house LPTN analysis tools for rotating machines at ABB. Temperature results from the LPTN calculations were compared with measured values. The comparison indicated satisfactory performance for the available measurements.

Conclusions and outlook

In section 2.6 the question *Can numerical methods be applied for understanding heat transfer on such a detailed level that flow structures causing heat transfer can be understood?* was introduced. The study presented in **paper 2** and **paper 3** indicates a positive answer to the question. The simulation approach chosen produces data which can be processed to correlate flow structures with heat transfer structures. For the configuration considered in these papers the simulation approach chosen renders averaged heat transfer results which are close to published values obtained through experiments for a similar system. The results indicate that the methods can be considered for application in studies of heat transfer in electric machine oriented configurations. Naturally, thought need to be put into extracting and resolving a relevant portion which is of computationally manageable size.

The other question presented in section 2.6 was *Which approaches can be applied to improve the predictive capability of thermal analysis tools employed in industry?*. The content of **paper 1** indicates that care should be taken when considering where in the machine temperature sensors should be placed if the data is intended for comparison with simulations which resolves the machine in three spatial dimensions. Ideally an iterative approach between simulation model development and actual machine prototype development could be envisioned. Following such an approach strictly is rarely realizable, but creative thinking can likely identify an equally good approach which can be executed given a sufficient time frame. The prototyped method presented in **paper 4** show that there is potential in developing this approach further. An automated method for adjusting thermal network definitions based on external temperature input could aid in development or refinement of cooling features, as the influence these bring can be brought into the simulation models, from experimental testing, for further evaluations. The work is at an early stage and more development remain to assess the real-world usability of this approach. Additionally, other computational methods for the adjustments can be considered. **Paper 5** shows how CFD can be employed to generate input-data, associated with a subsection of a machine, that can be used in LPTN analysis of the full machine system. This is an efficient first step, or complement, to full parameter span experiments. The suggestions that can be

given towards finding an answer to the posed question can be summarized as: consider sensor placement when evaluating the simulation performance, consider further development of automated model adjustment approaches, and when the heat transfer behavior is unknown consider employing CFD for complementing the input data.

Acknowledgements

The work was funded by the Swedish Foundation for Strategic Research and ABB. Simulations were performed on computational resources provided by ABB AB, Corporate Research, in Västerås, Sweden.

Thanks to Panagiotis Kakosimos, Simon Lundberg, Anders Dahlkild, Binaya Baidar, and Christophe Duwig for providing useful comments and suggestions during the authoring of this work.

Thanks to advance reviewer Jens Fridh for reading the text and providing concrete and actionable feedback. Thanks to Magnus Backman and Dmitry Svechkarenko for reading the manuscript in detail and providing suggestions for improvements.

Thanks to the industrial supervisors, past and present, Luca Peretti, Rebei Bel-Fdhila, and Zlatko Kolondjovski.

Bibliography

- AARNIOVUORI, L., NIEMELA, M., PYRHONEN, J., CAO, W. & AGAMLOH, E. B. 2018 Loss components and performance of modern induction motors. In *Proceedings - 2018 23rd International Conference on Electrical Machines, ICEM 2018*, pp. 1253–1259.
- BALLESTÍN-BERNAD, V., ARTAL-SEVIL, J. S. & DOMÍNGUEZ-NAVARRO, J. A. 2021 A review of transverse flux machines topologies and design. *Energies (Basel)* **14** (21), 7173–.
- BECKLEY, P. 2002 *Electrical Steels for Rotating Machines. IEE power and energy series*. Stevenage: The Institution of Engineering and Technology.
- BENNER, P., GRIVET-TALOCIA, S., QUARTERONI, A., GIANLUIGI ROZZA, W. S. & SILVEIRA, L. M., ed. 2020a *Model Order Reduction - Volume 2: Snapshot-Based Methods and Algorithms*. Berlin, Boston: De Gruyter.
- BENNER, P., GRIVET-TALOCIA, S., QUARTERONI, A., GIANLUIGI ROZZA, W. S. & SILVEIRA, L. M., ed. 2020b *Model Order Reduction - Volume 3: Applications*. Berlin, Boston: De Gruyter.
- BENNER, P., GRIVET-TALOCIA, S., QUARTERONI, A., GIANLUIGI ROZZA, W. S. & SILVEIRA, L. M., ed. 2021 *Model Order Reduction - Volume 1: System- and Data-Driven Methods and Algorithms*. Berlin, Boston: De Gruyter.
- BERGMAN, T., LAVINE, A., INCROPERA, F. & DEWITT, D. 2017 *Fundamentals of Heat and Mass Transfer*. Wiley.
- BOGLIETTI, A. & CAVAGNINO, A. 2007 Analysis of the endwinding cooling effects in TEFC induction motors. *IEEE transactions on industry applications* **43** (5), 1214–1222.
- BOGLIETTI, A., CAVAGNINO, A., STATON, D., POPESCU, M., COSSAR, C. & MCGILP, M. 2009 End space heat transfer coefficient determination for different induction motor enclosure types. *IEEE transactions on industry applications* **45** (3), 929–937.
- BOGLIETTI, A., COSSALE, M., POPESCU, M. & STATON, D. A. 2019 Electrical machines thermal model: Advanced calibration techniques. *IEEE transactions on industry applications* **55** (3), 2620–2628.
- BOLAM, R. C., VAGAPOV, Y. & ANUCHIN, A. 2018 Review of electrically powered propulsion for aircraft. In *Proceedings - 2018 53rd International Universities Power Engineering Conference, UPEC 2018*.
- BOLDEA, I. 2013 *Linear electric machines, drives, and MAGLEVs handbook*, 1st edn. Boca Raton: CRC Press.

- BORTONI, E. D. C. 2009 Are my motors oversized? *Energy conversion and management* **50** (9), 2282–2287.
- BORÉE, J. 2003 Extended proper orthogonal decomposition : a tool to analyse correlated events in turbulent flows. *Experiments in Fluids* **35**, 188–192.
- BUCKINGHAM, E. 1914 On physically similar systems: Illustrations of the use of dimensional equations. *Physical review* **4** (4), 345–376.
- BURESTI, G. 2015 A note on stokes' hypothesis. *Acta mechanica* **226** (10), 3555–3559.
- CAPEHART, B. L., KENNEDY, W. J. & TURNER, W. C. 2020 *Guide to Energy Management, Eighth Edition - International Version*. Milton: River Publishers.
- EU C/2019/2125 2019-10-25 Commission regulation (eu) 2019/1781 of 1 october 2019 laying down ecodesign requirements for electric motors and variable speed drives pursuant to directive 2009/125/ec of the european parliament and of the council, amending regulation (ec) no 641/2009 with regard to ecodesign requirements for glandless stand-alone circulators and glandless circulators integrated in products and repealing commission regulation (ec) no 640/2009. *OJ L* **272**, 74–94.
- FASIL, M., PLESNER, D., WALTHER, J. H., MIJATOVIC, N., HOLBØLL, J. & JENSEN, B. B. 2014 Numerical and experimental investigation of heat flow in permanent magnet brushless dc hub motor. *SAE International Journal of Alternative Powertrains* **4** (1), 46–57.
- FERZIGER, J. H. 2002 *Computational methods for fluid dynamics*, 3rd edn. Berlin: Springer.
- FERZIGER, J. H. 2020 *Computational Methods for Fluid Dynamics*, 4th edn. Cham: Springer International Publishing.
- GARNIER, E., ADAMS, N. & SAGAUT, P. 2009 *Large Eddy Simulation for Compressible Flows. Scientific Computation*. Dordrecht: Springer Netherlands.
- GE, B., ZHANG, J. & TAO, D. 2022 Thermal analysis of axial-radial hybrid ventilation motor and stator ventilation channel improvement. *IET Electric Power Applications* **16** (11), 1330–1338.
- GHAHFAROKHI, P. S., KALLASTE, A., PODGORNOVS, A., BELAHČEN, A. & VAIMANN, T. 2020 Development of analytical thermal analysis tool for synchronous reluctance motors. *IET electric power applications* **14** (10), 1828–1836.
- GILSON, G., PICKERING, S., HANN, D. & GERADA, C. 2009 Analysis of the end winding heat transfer variation with altitude in electric motors. In *2009 35th Annual Conference of IEEE Industrial Electronics*, pp. 2545–2550. IEEE.
- GINET, C., JOHO, R. & VERRIER, M. 2007 The turbogenerator - a continuous engineering challenge. In *2007 IEEE Lausanne Power Tech*, pp. 1055–1060. IEEE.
- GLEW, N. 1999 Design and manufacture of energy efficient and environmentally friendly large machines. *IEE Colloquium (Digest)* (178), 1–5.
- HAN, J., JIECHEN, D., WANG, Y., WANG, C., GE, B. & LI, W. 2021 Coupled electromagnetic-fluid-thermal analysis for end zone with electric screen in large water-hydrogen-hydrogen cooled turbine generator under different end winding extensions. *IEEE transactions on energy conversion* **36** (4), 2703–2713.
- IEA 2019 *World Energy Outlook 2019*. Paris: OECD Publishing.
- IEA 2021a *Net Zero by 2050*. Paris: IEA.
- IEA 2021b *World Energy Outlook 2021*. Paris: OECD Publishing.
- IEC 1991 Rotating electrical machines – Part 6: Methods of cooling. Standard

- CEI/IEC 34-6:1991. International Electrotechnical Commission (IEC), Geneva, CH.
- IEC 2007 Electrical insulation – Thermal evaluation and designation. Standard. International Electrotechnical Commission (IEC), Geneva, CH.
- IEC 2022*a* Magnetic materials – Part 8-4: Specifications for individual materials - Cold-rolled non-oriented electrical steel strip and sheet delivered in the fully-processed state. Standard. International Electrotechnical Commission (IEC), Geneva, CH.
- IEC 2022*b* Rotating electrical machines – Part 6: Rating and performance. Standard. International Electrotechnical Commission (IEC), Geneva, CH.
- IPCC 2022 Climate change 2022: Mitigation of climate change. contribution of working group iii to the sixth assessment report of the intergovernmental panel on climate change. *Tech. Rep.*. IPCC, Cambridge, United Kingdom and New York, NY, USA.
- JOHN R. RUMBLE, ED. 2022 Thermal and physical properties of pure elemental metals. In *CRC Handbook of Chemistry and Physics*, 103rd Edition (Internet Version 2022) edn. (ed. J. R. Rumble). CRC Press/Taylor & Francis.
- KAHOURZADE, S., MAHMOUDI, A., PING, H. W. & UDDIN, M. N. 2014 A comprehensive review of axial-flux permanent-magnet machines. *Canadian journal of electrical and computer engineering* **37** (1), 19–33.
- KANDLIKAR, S., GARIMELLA, S., LI, D., COLIN, S. & KING, M. 2014 *Heat transfer and fluid flow in minichannels and microchannels*, 2nd edn. Oxford : Butterworth-Heinemann.
- KRINGS, A. 2014 Iron losses in electrical machines - influence of material properties, manufacturing processes, and inverter operation. PhD thesis, KTH, Electrical Energy Conversion, qC 20140516.
- KRINGS, A. & SOULARD, J. 2010 Overview and comparison of iron loss models for electrical machines. *Journal of Electrical Engineering* **10** (3), 162–.
- KRSTIC, M. 2006 Chapter 9 - mixing control for jet flows. In *Combustion Processes in Propulsion* (ed. G. D. Roy), pp. 87–96. Burlington: Butterworth-Heinemann.
- LANDAU, L. D. & LIFSHITZ, E. M. 1987 *Fluid mechanics*, 2nd edn. Oxford: Pergamon Press.
- LI, W., SU, Y., LI, D., LI, Y., HU, L. & WANG, P. 2019 Multi-physical fields of rotor windings with axial-radial ventilation system for 1100 mw nuclear half-speed turbine generator. *Energy (Oxford)* **188**, 116092.
- LIANG, D., ZHU, Z., ZHANG, Y., FENG, J., GUO, S., LI, Y., WU, J. & ZHAO, A. 2021 A hybrid lumped-parameter and two-dimensional analytical thermal model for electrical machines. *IEEE transactions on industry applications* **57** (1), 246–258.
- LIENHARD, IV, J. H. & LIENHARD, V, J. H. 2020 *A Heat Transfer Textbook*, 5th edn. Cambridge, MA: Phlogiston Press, version 5.10.
- LIPO, T. A. 2017 *Introduction to AC machine design. IEEE Press series on power engineering* . Hoboken, New Jersey: Wiley.
- MADONNA, V., WALKER, A., GIANGRANDE, P., SERRA, G., GERADA, C. & GALEA, M. 2019 Improved thermal management and analysis for stator end-windings of electrical machines. *IEEE transactions on industrial electronics (1982)* **66** (7), 5057–5069.

- MELLOR, P. H., ROBERTS, D. & TURNER, D. R. 1991 Lumped parameter thermal model for electrical machines of TEFC design. *IEE proceedings. Part B, Electric power applications* **138** (5), 205–218.
- MENTER, F. R. 1994 Two-equation eddy-viscosity turbulence models for engineering applications. *AIAA journal* **32** (8), 1598–1605.
- MENTER, F. R., FERREIRA, J. C., ESCH, T. & KONNO, B. 2003a The sst turbulence model with improved wall treatment for heat transfer predictions in gas turbines.
- MENTER, F. R., KUNTZ, M. & LANGTRY, R. 2003b Ten years of industrial experience with the sst turbulence model.
- MOSES, A., ANDERSON, P., JENKINS, K. & STANBURY, H. 2019a *Electrical Steels: Fundamentals and basic concepts, Volume 1: Fundamentals and basic concepts, Volume 1*. Stevenage: The Institution of Engineering and Technology.
- MOSES, A., ANDERSON, P., JENKINS, K. & STANBURY, H. 2019b *Electrical Steels: Performance and applications, Volume 2: Performance and applications, Volume 2*. Stevenage: The Institution of Engineering and Technology.
- NAGAKURA, K., OTAKA, T., KAKIUCHI, M., GUNJI, Y., NAKAYAMA, S., MURATA, D., KABATA, Y. & HATANO, H. 2009 Development of the world's largest hydrogen indirectly cooled turbine generator. In *2009 International Conference on Electrical Machines and Systems*, pp. 1–6. IEEE.
- NAGEL, L. W. & PEDERSON, D. O. 1973 Spice (simulation program with integrated circuit emphasis).
- NCFMF 1972 Illustrated experiments in fluid mechanics - the NCFMF book of film notes. <http://web.mit.edu/hml/ncfmf.html>.
- ORLOVA, S., RASSÖLKIN, A., KALLASTE, A., VAIMANN, T. & BELAHCEN, A. 2016 Lifecycle analysis of different motors from the standpoint of environmental impact. *Latvian journal of physics and technical sciences* **53** (6), 37–46.
- PAPKOV, A., MEL'NICHENKO, A., PAK, V. & KUIMOV, I. 2007 New electric insulating materials for the insulation systems of rotating electrical machines. *Russian electrical engineering* **78** (3), 149–155.
- PEDREGOSA, F., VAROQUAUX, G., GRAMFORT, A., MICHEL, V., THIRION, B., GRISEL, O., BLONDEL, M., PRETTENHOFER, P., WEISS, R., DUBOURG, V., VANDERPLAS, J., PASSOS, A., COURNAPEAU, D., BRUCHER, M., PERROT, M. & DUCHESNAY, E. 2011 Scikit-learn: Machine learning in Python. *Journal of Machine Learning Research* **12**, 2825–2830.
- POINSOT, T. 2001 *Theoretical and numerical combustion*. Philadelphia, Pa.: Edwards.
- PYRHONEN, J., JOKINEN, T. & HRABOVCOVÁ, V. 2014 *Design of rotating electrical machines*, second edition. edn. Chichester, West Sussex, United Kingdom: Wiley.
- QUARTERONI, A. 2017 *Numerical Models for Differential Problems*, 3rd edn. *MS&A, Modeling, Simulation and Applications, 16*. Cham: Springer International Publishing.
- RÖNNBERG, K. 2020 Heat-transfer simulations applied to electrical machines. <http://urn.kb.se/resolve?urn=urn:nbn:se:kth:diva-286686>.
- SAIDUR, R. 2010 A review on electrical motors energy use and energy savings. *Renewable & sustainable energy reviews* **14** (3), 877–898.
- SALVAIRE, F. 2021 Pyspice. <https://pyspice.fabrice-salvaire.fr>.
- STATON, D., CHONG, E., PICKERING, S. & BOGLIETTI, A. 2022 *Cooling of rotating*

- electrical machines : Fundamentals, modelling, testing and design.*, 1st ed.. edn. *Energy Engineering ser 1*. IET.
- STONE, G. C., CULBERT, I., BOULTER, E. A. & DHIRANI, H. 2014 *Electrical Insulation for Rotating Machines: Design, Evaluation, Aging, Testing, and Repair*, 2nd edn. *IEEE Press Series on Power Engineering* . Somerset: Wiley.
- TATA STEEL - SURAHAMMARS BRUK 2022 Typical data for SURA[®] M270-50A. <https://www.tatasteeleurope.com/ts/sites/default/files/M270-50A.pdf>.
- VAN DYKE, M. 1982 *An album of fluid motion*. Stanford: The Parabolic press.
- VDI GESELLSCHAFT 2010 *VDI Heat Atlas*. Berlin, Heidelberg: Springer Berlin / Heidelberg.
- VERSTEEG, H. K. 2007 *An introduction to computational fluid dynamics : the finite volume method*, 2nd edn. Harlow: Pearson Prentice Hall.
- WANG, X., LI, B., GERADA, D., HUANG, K., STONE, I., WORRALL, S. & YAN, Y. 2022 A critical review on thermal management technologies for motors in electric cars. *Applied thermal engineering* **201**, 117758–.
- WELLER, H. G., TABOR, G., JASAK, H. & FUREBY, C. 1998 A tensorial approach to computational continuum mechanics using object-oriented techniques. *Computers in Physics* **12** (6), 620–631.
- WILCOX, D. C. 2006 *Turbulence modeling for CFD*, 3rd edn. La C nada, Calif.: DCW Industries.
- ZIENKIEWICZ, O. C. 2014 *The finite element method for fluid dynamics*, seventh edition. edn. Amsterdam: Elsevier/Butterworth-Heinemann.

Part II

Papers

Summary of the papers

Paper 1

Thermal Modelling of Totally Enclosed Fan Cooled motors

This paper deals with thermal simulations of an electric motor for traction applications. The motor is designed with several axial cooling channels in which air, supplied by a shaft mounted fan, flows. Several simulations are performed with different definitions of the loss distribution in the machine, combined with different definitions of the air distribution in the axial channels. The results are compared with experimentally obtained data, showing how the different simulation results compare with full-load operation at 4800rpm.

Paper 2

Large Eddy Simulation of circular impinging jet for heat transfer applications

Simulations of heat transfer resulting from a jet impinging on a flat plate is presented in this paper. A Large-Eddy Simulation approach employing the Wall-Adapting Local Eddy-viscosity subgrid scale model. Simulation results are compared with published experimental data and correlations. Heat transfer resulting from different inlet velocity profiles were considered.

Paper 3

Heat transfer and associated coherent structures of a single impinging jet from around nozzle

In this paper the heat transfer from a single round impinging jet is analyzed in detail through simulations. A LES simulation approach together with the WALE subgrid scale model is employed. The impact on the resulting heat transfer from employing a constant temperature or constant heat flux boundary condition at the plate is studied. A statistical analysis on the resulting heat transfer for a selected case indicate that the Nusselt-number follow a gamma-distribution. POD on the heat transfer field is employed and the results are linked to the flow field through EPOD. POD showed low relative strength in the dominating modes, yet distinct shapes to the spatial basis function. The associated flow field, identified through EPOD, showed distinct flow features for the low order modes.

Paper 4*Machine Learning-Based Adjustments Of Thermal Networks*

In this paper an approach to automated adjustments of Lumped Parameter Thermal Network definitions is presented. The adjustments are made on the LPTN parameters with the intention to minimize the difference between the LPTN prediction and an input temperature field. A thermal network describing a half-tooth-half-slot is defined and used for building a training database and for defining test cases used for assessing the performance of the approach. For the selected thermal network and the selected cases the evaluation indicate promising performance.

Paper 5*Analysis of end winding heat transfer in a low-speed motor with forced external cooling*

In totally enclosed machines the air flow inside the machine is in most cases driven by the rotor shaft. This arrangement is very common on low voltage machines for industrial applications. In this paper the combined effect of rotor rotation and a forced cooling component on the heat transfer at the end winding of a form-wound machine is studied through simulations. The obtained results were used for extending a correlation used for pure rotor driven flows to include the effect of the externally supplied coolant flow. The correlation was implemented in an in-house lumped parameter thermal network analysis tool, developed for rotating machine thermal analysis, and results compared to experiments. The comparison shows promising performance.